Sustainable Food Technology

ROYAL SOCIETY OF CHEMISTRY

PAPER

View Article Online
View Journal

Cite this: DOI: 10.1039/d5fb00655d

Ultrasound-assisted extraction of mangiferin from *Mangifera pajang* Kosterm. fruit using a choline chloride-based natural deep eutectic solvent: optimisation and antidiabetic activity

Muhammad Daniel Eazzat Mohd Rosdan, [a] Mohd Azrie Awang, *[ab] Mohammad Amil Zulhilmi Benjamin, [c] Aniza Saini, [a] Muhammad Naufal Qaweim Rushdy [a] and Hasdian Mudin [a]

The growing demand for sustainable bioresources has highlighted the importance of exploring underutilised plant species as alternative sources of health-promoting compounds. *Mangifera pajang* Kosterm. (bambangan), an endemic and underexploited fruit native to Borneo, particularly Sabah, Malaysia, offers considerable potential as a sustainable source of bioactive constituents. However, research on efficient extraction techniques and processing technologies to recover its valuable phytochemicals remains limited. In this study, *M. pajang* fruit was pretreated using ultrasound-assisted osmotic dehydration (UAOD), and the one-factor-at-a-time (OFAT) method was subsequently used for parameter screening, followed by a response surface methodology with central composite design to optimise ultrasound-assisted extraction using a natural deep eutectic solvent (NADES). Parameters including extraction time, solid-to-solvent ratio, and ultrasonic amplitude were evaluated to maximise total phenolic content (TPC), total flavonoid content (TFC), and mangiferin content. Bioactivity was assessed through antioxidant and antidiabetic assays based on IC_{50} values of the optimised *M. pajang* fruit extract (MPFE) compared with positive controls. Molecular docking was performed against α-glucosidase. ADMET and drug-likeness were predicted to evaluate the potential pharmacokinetic behaviour and oral drug-likeness properties of mangiferin. The optimised conditions were an extraction time of 11.33 min, a solid-to-solvent ratio of 1 : 28.52 g mL^{-1}, and an ultrasonic amplitude of 51.41%, achieving 53.02 ± 1.57 mg GAE g^{-1} TPC, 17.26 ± 1.13 mg RE g^{-1} TFC, and 0.66 ± 0.01 mg g^{-1} mangiferin. *In vitro*, the MPFE exhibited antioxidant (IC_{50} = 117.58 ± 2.19 μg mL^{-1}) and antidiabetic (IC_{50} = 90.54 ± 1.60 μg mL^{-1}) activities. *In silico*, mangiferin (−8.0 kcal mol^{-1}) showed stronger binding affinity to α-glucosidase compared with acarbose (−7.3 kcal mol^{-1}). ADMET and drug-likeness prediction further revealed that mangiferin showed higher intestinal absorption, better renal clearance, fewer rule violations, and stronger membrane permeability than acarbose, although solubility was lower. These findings suggest that *M. pajang* fruit represents a promising sustainable source of nutraceuticals and functional food products for managing oxidative stress and diabetes, although further experimental validation remains necessary.

Received 6th October 2025
Accepted 17th May 2026

DOI: 10.1039/d5fb00655d

rsc.li/susfoodtech

Sustainability spotlight

This study promotes the sustainable utilisation of *Mangifera pajang*, an underutilised indigenous fruit from Borneo, through a green ultrasound-assisted extraction process using a choline chloride-based natural deep eutectic solvent (NADES). By optimising the extraction of bioactive mangiferin, this work supports waste valorisation and local biodiversity utilisation while reducing environmental impact. The use of a NADES also supports an eco-friendly, low-toxicity, and potentially recyclable solvent system, in line with the United Nations Sustainable Development Goals, particularly SDG 3 (Good Health and Well-being) and SDG 12 (Responsible Consumption and Production). Overall, this research highlights the potential of *M. pajang* as a sustainable source of natural antioxidant and antidiabetic compounds for functional food and nutraceutical applications.

[a]*Faculty of Food Science and Nutrition, Universiti Malaysia Sabah, Jalan UMS, 88400 Kota Kinabalu, Sabah, Malaysia*

[b]*Food Security Research Laboratory, Faculty of Food Science and Nutrition, Universiti Malaysia Sabah, Jalan UMS, 88400 Kota Kinabalu, Sabah, Malaysia. E-mail: ma.awang@ums.edu.my*

[c]*Institute for Tropical Biology and Conservation, Universiti Malaysia Sabah, Jalan UMS, 88400 Kota Kinabalu, Sabah, Malaysia*

1 Introduction

Recently, natural deep eutectic solvents (NADES), also referred to as green solvents, have gained significant attention, with numerous combinations of hydrogen bond acceptors (HBAs) and hydrogen bond donors (HBDs) being investigated for their effectiveness in extracting phytochemicals from plants.[1,2] Beyond their rapid preparation, NADES offer a simple, energy-efficient, waste-reducing, and environmentally friendly approach to extraction.[3] Ultrasound-assisted extraction (UAE) is another green extraction technique that promotes the disruption of plant cell walls, thereby enhancing the solubility of bioactive compounds and increasing the yield of phenolic and flavonoid compounds.[4] In addition, the response surface methodology (RSM) is a valuable statistical tool for analysing complex interactions between factors (independent variables) and responses (dependent variables) to optimise targeted outcomes.[5] Within the RSM, central composite design (CCD) strengthens factorial design by incorporating centre and axial points to estimate curvature effects on the response surface.[6] The inclusion of multiple centre points further improves the prediction accuracy within the design space.[7]

Diabetes mellitus is a chronic disease characterised by insufficient insulin production by the pancreas or the ineffective utilisation of insulin by the body.[8] In Malaysia, the prevalence of diabetes among adults aged 20–79 has increased from 16.8% to 19.9% in 2024.[9,10] This rising trend reflects the growing public health burden of diabetes in the country. In parallel, there is increasing global interest in phytochemicals derived from medicinal plants and wild fruits, driven by consumer preference for natural products.[11] Plant-derived bioactive compounds offer several advantages over synthetic drugs, including fewer side effects, better patient tolerance, lower costs, and renewable sources.[12] Standardisation of extraction processes is therefore essential to ensure consistent levels of active compounds, thus helping to guarantee the efficacy and quality of plant-based therapeutics. Among promising natural resources, *Mangifera pajang* Kosterm., known locally as bambangan, is a wild fruit native to Sabah, Malaysia, belonging to the Anacardiaceae family. It contains diverse phytochemicals, such as polyphenols, flavonoids, carotenoids, and anthocyanins, which contribute to its pharmacological activities, including antioxidant, antibacterial, anticancer, antidiabetic, and cytoprotective effects.[13,14] Mangiferin, one of the main phenolic compounds in *M. pajang*, has demonstrated antidiabetic, antitumour, and immunomodulatory activities.[15] Lasano *et al.*[16] further reported its potential as a novel agent in diabetes management. Moreover, pretreatments such as ultrasound-assisted osmotic dehydration (UAOD) have been shown to enhance the preservation of bioactive compounds, improve product quality, and increase the extraction efficiency while remaining cost-effective.[17]

To the best of our knowledge, no prior studies have investigated the optimisation of the total phenolic content (TPC), total flavonoid content (TFC), and mangiferin content from a pretreated *M. pajang* fruit extract (MPFE) using UAE. Furthermore, the biological properties of the optimised extract have not been comprehensively assessed through both *in vitro* (antioxidant and antidiabetic assays) and *in silico* approaches, including molecular docking, drug-likeness, and ADMET (absorption, distribution, metabolism, excretion, and toxicity), which are crucial for evaluating its potential antioxidant and antidiabetic effects. Therefore, this study aimed to optimise the extraction of MPFE with respect to TPC, TFC, and mangiferin content, followed by evaluation of its antioxidant and antidiabetic properties. The findings provide new insights into the potential of this underutilised local fruit as a sustainable resource for nutraceutical and functional food development.

2 Materials and methods

2.1 Preparation of raw materials with UAOD

M. pajang fruits were obtained from local vendors in Anjung Kinabalu, Kota Kinabalu, Sabah, Malaysia. Approximately 100 g of sliced fruit pulp was soaked in a 30% sugar solution and subsequently subjected to UAOD using an ultrasonic water bath (CPX8800H, Branson, Brookfield, CT, USA) operating at 40 kHz and 320 W, and maintained at 50 °C for 60 min. The treated samples were then dried in an oven (ED 23, Binder, Tuttlingen, Germany) at 50 °C for 6 h. The dried samples were ground into a fine powder (60 mesh, 0.30 mm) using a grinder (EBM-9182, Elba, Borso del Grappa, Italy) and stored in airtight amber glass containers at room temperature (23 °C) in a dark environment until further analysis. The procedure was adapted, with minor modifications, from the methods described by Mohd Rosdan *et al.*[18] and Abrahão *et al.*[19]

2.2 Preparation of NADES

NADES was prepared using choline chloride as the HBA and lactic acid as the HBD at a molar ratio of 1 : 2 (87 g of choline chloride and 113 g of lactic acid for the preparation of 200 g), following the heating and stirring method with slight modifications.[20] The mixture, containing deionised water, was heated at 70 °C with continuous magnetic stirring until a uniform and transparent solution was obtained, which required approximately 30 min. The prepared NADES was then stored at room temperature until further use.

2.3 Screening and optimisation of the extraction process

Extraction of MPFE was carried out using a probe sonicator (Q500 Sonicator, QSonica, Newtown, CT, USA) equipped with a 13 mm diameter probe in a NADES medium, following the method described by Zulkifli *et al.*[21] with minor modifications. The extraction process was examined using a two-stage approach, beginning with one-factor-at-a-time (OFAT) screening of four key parameters, namely extraction time (5–25 min), solid-to-solvent ratio (1 : 10–1 : 50 g mL^{-1}), ultrasonic amplitude (30–70%), and duty cycle (74.07–86.96%), using a NADES as the extraction medium.[22] The screening was initiated under fixed conditions of 15 min extraction time, a solid-to-solvent ratio of 1 : 30 g mL^{-1}, an ultrasonic amplitude of 50%, and a duty cycle of 80.00% (20 s on and 5 s off). Under

these conditions, the solid-to-solvent ratio was varied from 1 : 10 to 1 : 50 g mL^{-1}.[23] Duty cycle ranges were then set at 74.07%, 76.92%, 80.00%, 83.33%, and 86.96%, with the solid-to-solvent ratio (1 : 30 g mL^{-1}), ultrasonic amplitude (50%), and extraction time (15 min) held constant. For these tests, the "on" time of the duty cycle was fixed at 20 s, while the "off" time varied from 3 to 7 s.[24] The duty cycle was determined using eqn (1), adapted from Lanjekar *et al.*[25] Next, extraction time was varied from 5 to 25 min while maintaining a solid-to-solvent ratio of 1 : 30 g mL^{-1}, an ultrasonic amplitude of 50%, and a duty cycle of 86.96% (20 s on and 3 s off).[26] Finally, the ultrasonic amplitude was tested within the range of 30–70%, while the solid-to-solvent ratio (1 : 30 g mL^{-1}), duty cycle (86.96%), and extraction time (10 min) were kept constant.[27] These parameters were selected based on evidence from previous studies, which reported their significant influence on TPC, TFC, and bioactive compound recovery.[28] After extraction, solid residues were removed by vacuum filtration through Whatman No. 1 filter paper. The resulting filtrates were stored at 4 °C until further analysis. All results are expressed on a dry weight (DW) basis to ensure standardisation of the measurements.

$$\text{Duty cycle}(\%) = \frac{\text{ON time(s)}}{\text{ON time(s)} + \text{OFF time(s)}} \times 100 \quad (1)$$

Table 1 Factors and coded levels used in MPFE extraction

		Levels (coded)		
Factors	Code	−1	0	1
Extraction time (min)	*A*	5	10	15
Solid-to-solvent ratio (g mL^{-1})	*B*	1 : 20	1 : 30	1 : 40
Ultrasonic amplitude (%)	*C*	40	50	60

Based on the significant parameters identified during preliminary screening, three factors with three levels each were selected for further optimisation using RSM-CCD in Design-Expert version 13. The selected parameters and their corresponding levels are presented in Table 1, while the CCD experimental design consisting of 17 runs is shown in Table 2. Actual values obtained from these runs were compared with model-predicted values to validate the statistical optimisation. Model performance was assessed using one-way analysis of variance (ANOVA), with significance determined at $p < 0.05$, together with fit statistics including the coefficient of variation (CV), coefficient of determination (R^2), adjusted and predicted R^2 values, and adequate precision.

2.4 Determination of TPC

The MPFE was determined *via* the Folin–Ciocalteu method, as adapted from Mudin *et al.*[29] with minor modifications. A 100 μL aliquot of the sample extract was mixed with 500 μL of Folin–Ciocalteu reagent and 1.5 mL of 20% sodium carbonate solution, and the final volume was adjusted to 10 mL with ultrapure water. The mixture was incubated in the dark at room temperature for 2 h. The absorbance was measured at 765 nm using a UV-vis spectrophotometer (Lambda 25, PerkinElmer, Waltham, MA, USA). Gallic acid served as the standard, and the results were expressed as mg GAE/g DW based on eqn (2).

$$\text{Total phenolic content}\left(\text{mg GAE g}^{-1}\text{DW}\right) = \frac{c \times V}{m} \quad (2)$$

where c represents the concentration of liquid extract (mg mL^{-1}) obtained from the standard curve of TPC, V represents the solvent volume (mL), and m represents the mass of dried plant material (g).

Table 2 RSM-CCD design matrix with factors and response variables for MPFE extraction

	Factors			Responses		
	Extraction time (min)	Solid-to-solvent ratio (g mL^{-1})	Ultrasonic amplitude (%)			
Run	*A*	*B*	*C*	Total phenolic content (mg GAE g^{-1})	Total flavonoid content (mg RE g^{-1})	Mangiferin content (mg g^{-1})
1	15	40	60	25.45	6.96	0.45
2	5	20	40	55.31	16.88	0.65
3	5	40	60	32.36	9.15	0.27
4	18	30	50	22.49	5.66	0.39
5	15	20	60	28.40	6.63	0.28
6	15	20	40	39.62	12.16	0.17
7	10	30	33	32.91	11.76	0.56
8	10	30	50	29.40	7.20	0.59
9	10	13	50	29.69	8.02	0.29
10	5	20	60	33.56	7.77	0.01
11	10	30	67	24.85	7.61	0.37
12	15	40	40	33.95	11.11	0.65
13	10	30	50	33.14	9.28	0.19
14	5	40	40	38.74	11.19	0.44
15	10	30	50	37.36	10.94	0.52
16	10	47	50	56.28	16.47	0.62
17	2	30	50	54.29	15.90	0.61

2.5 Determination of TFC

The MPFE was assessed using the aluminium chloride colorimetric assay according to Jinin *et al.*[30] with slight alterations, in which 1 mL of MPFE was mixed with 1 mL of 2% aluminium chloride solution. The mixture was incubated in the dark at room temperature for 15 min. The absorbance was measured at 430 nm using a UV-vis spectrophotometer, and rutin served as the standard. The results were expressed as mg RE g^{-1} DW based on eqn (3).

$$\text{Total flavonoid content}\left(\text{mg RE g}^{-1}\text{DW}\right) = \frac{c \times V}{m} \quad (3)$$

where c represents the concentration of liquid extract (mg mL^{-1}) obtained from the standard curve of TFC, V represents the solvent volume (mL), and m represents the mass of dried plant material (g).

2.6 Determination of mangiferin content

The MPFE (1 mg mL^{-1}) was dissolved in deionised water, while the mangiferin standard (1 mg mL^{-1}) was dissolved in methanol and prepared at concentrations ranging from 20 to 100 ppm. All solutions were filtered through a 0.22 μm membrane filter prior to analysis. High-performance liquid chromatography was performed using an Agilent 1100 system (Agilent Technologies, Santa Clara, CA, USA) equipped with an InertSustain C18 column (5 μm, 150 × 4.6 mm) and a UV-vis detector. The injection volume was 20 μL, with a total run time of 15 min, a flow rate of 0.8 mL min^{-1}, and detection at 254 nm. An isocratic elution was applied, with mobile phase A consisting of 0.1% formic acid in deionised water and mobile phase B consisting of acetonitrile. This method was adapted, with slight modifications, from Mohd Rosdan *et al.*[18] Mangiferin content was calculated using eqn (4).

$$\text{Mangiferin content}\left(\text{mg g}^{-1}\right) = \frac{\text{Mass of mangiferin (mg)}}{\text{Dried mass of plant material(g)}} \quad (4)$$

2.7 Determination of bioactivity

2.7.1 *In vitro* DPPH inhibition assay. The 2,2-diphenyl-1-picrylhydrazyl (DPPH) radical scavenging activity was determined following the method of Saini *et al.*[31] with minor modifications. Solutions of optimised MPFE were prepared at concentrations of 5, 10, 20, 40, 60, 80, 100, 200, 400, 600, 800, and 1000 μg mL^{-1}, while standard solutions of mangiferin and ascorbic acid were prepared at concentrations of 5, 10, 20, 40, 60, 80, and 100 μg mL^{-1}. Briefly, 1 mL of MPFE was mixed with 1 mL of 0.1 mM DPPH solution and incubated in the dark for 30 min. Absorbance was measured at 517 nm using a UV-vis spectrophotometer. The negative control consisted of a DPPH solution without sample extract, while ascorbic acid was used as a positive control. The percentage of DPPH radical scavenging activity was calculated according to eqn (5).

$$\text{DPPH inhibition activity}(\%) = \frac{A_c - A_s}{A_c} \times 100 \quad (5)$$

where A_c represents the absorbance of the control and A_s represents the absorbance of the sample. The results were expressed as IC_{50} values (half-maximal inhibitory concentration), obtained through regression analysis, representing the concentration required to achieve 50% inhibition of radical scavenging activity.

2.7.2 *In vitro* α-glucosidase inhibition assay. The α-glucosidase inhibitory assay was conducted with slight modifications from previously described methods.[32] Solutions of optimised MPFE were prepared at concentrations of 5, 10, 15, 20, 25, 30, 50, 100, 150, 200, and 250 μg mL^{-1}, while standard solutions of mangiferin and acarbose were prepared at concentrations of 5, 10, 15, 20, and 25 μg mL^{-1}. The control solution was prepared without any inhibitors or samples, while acarbose was used as the positive control. The substrate used was 5 mM *p*-nitrophenyl-α-D-glucopyranoside (pNPG). Two buffers were used: Buffer I consisted of 0.1 M sodium phosphate buffer (pH 6.9) containing 2% dimethyl sulfoxide (DMSO), and Buffer II was 0.1 M sodium phosphate buffer (pH 6.9) without DMSO. Buffer I was used for diluting extracts and acarbose, whereas Buffer II was used for diluting the α-glucosidase enzyme and substrate.

The reaction mixture was prepared by combining 50 μL of sample solution with 50 μL of buffer, followed by the addition of 30 μL of α-glucosidase enzyme (1 U mL^{-1}). The mixture was incubated in a 96-well plate at 37 °C for 10 min. Subsequently, 20 μL of pNPG substrate was added, and the enzymatic reaction was allowed to proceed at 37 °C for 30 min. The release of *p*-nitrophenyl from pNPG was measured at 405 nm using a microplate reader (Multiskan SkyHigh, Thermo Fisher Scientific, Waltham, MA, USA). The percentage inhibition of α-glucosidase activity was calculated using eqn (6).

$$\text{α-Glucosidase inhibition activity}(\%) = \frac{A_c - A_s}{A_c} \times 100 \quad (6)$$

where A_c represents the absorbance of the control and A_s represents the absorbance of the sample. The results were expressed as IC_{50} values (half-maximal inhibitory concentration), obtained through regression analysis, representing the concentration required to achieve 50% inhibition of α-glucosidase activity.

2.7.3 *In silico* α-glucosidase inhibition assay. Molecular docking is a computational technique used to predict and visualise the binding interactions between ligands and protein receptors. The procedure followed the methods of Sabri *et al.*[33] and Sarkar *et al.*[34] The α-glucosidase enzyme (PDB ID: 5NN8) was retrieved from the RCSB Protein Data Bank and prepared by removing water molecules before docking. Mangiferin (PubChem ID: 5281647) was used as the target ligand, while acarbose (PubChem ID: 41774) served as the control ligand. Both ligands were obtained from the PubChem database and subsequently converted to Protein Data Bank (.pdb) format using BIOVIA Discovery Studio Visualizer version 4.0. Docking simulations were performed using the Cavity-Detection Guided Blind Docking (CB-Dock2) platform, which predicts potential binding cavities and provides binding affinity values for each ligand–protein interaction. The docking grid box was centred at the predicted catalytic cavity (Pocket C5) with coordinates

($x = -14$, $y = -32$, and $z = 64$) and a detected cavity volume of 401 Å^3. To accommodate the varying molecular sizes and ensure sufficient search space for conformational sampling and rotation, the grid dimensions were automatically set to 23 × 23 × 23 Å for mangiferin and 27 × 27 × 27 Å for acarbose. This adaptive sizing ensured that the entire active site was accessible while maintaining computational efficiency for each specific ligand–receptor complex.

2.8 ADMET and drug-likeness prediction

ADMET analysis is an important component of modern drug discovery, as it evaluates the pharmacokinetic properties of candidate compounds to predict their behaviour in biological systems, thereby enabling cost-effective screening.[35] The Simplified Molecular Input Line Entry System (SMILES) strings of the ligands were used as input for online prediction servers, including admetSAR 2.0, admetSAR 3.0, and SwissADME, to assess their ADMET characteristics.[36] Additionally, Osiris Property Explorer was employed to predict toxicity risks, while the drug-likeness evaluation was based on molecular weight (MW), HBD, HBA, partition coefficient ($c\log P$), number of Lipinski's Rule of Five (Ro5) violations, water solubility ($\log S$), and topological polar surface area (TPSA).

2.9 Statistical analysis

All experiments were conducted in independent biological triplicates ($n = 3$), and the results were expressed as mean ± standard deviation (SD). Statistical analysis was performed using ANOVA followed by Tukey's HSD post hoc test in GraphPad Prism version 10.4.0. A probability level of $p < 0.05$ was considered statistically significant.

3 Results and discussion

3.1 Parameter screening using OFAT

A preliminary study was conducted to establish the appropriate range of design parameters for optimising the extraction process using the OFAT method. Extraction is essential for recovering and isolating active compounds from plant materials, with the objective of maximising the TPC, TFC, and concentration of target substances.[37] The efficiency of extraction is affected by several factors, including solvent type, extraction time, solid-to-solvent ratio, ultrasonic amplitude, and duty cycle.[38,39] In this study, a NADES was selected as the extraction solvent and maintained as constant because it represents a greener alternative to conventional organic solvents such as methanol and ethanol, with advantages including lower toxicity, better environmental compatibility, and reduced dependence on volatile organic solvents, while still providing effective extraction of phytochemicals.[40] The screening parameters included extraction time, solid-to-solvent ratio, ultrasonic amplitude, and duty cycle (Fig. 1).

3.1.1 Effects of extraction time on TPC, TFC, and mangiferin content. The extraction time ranged from 5 to 25 min for TPC, TFC, and mangiferin content of MPFE, while the solid-to-

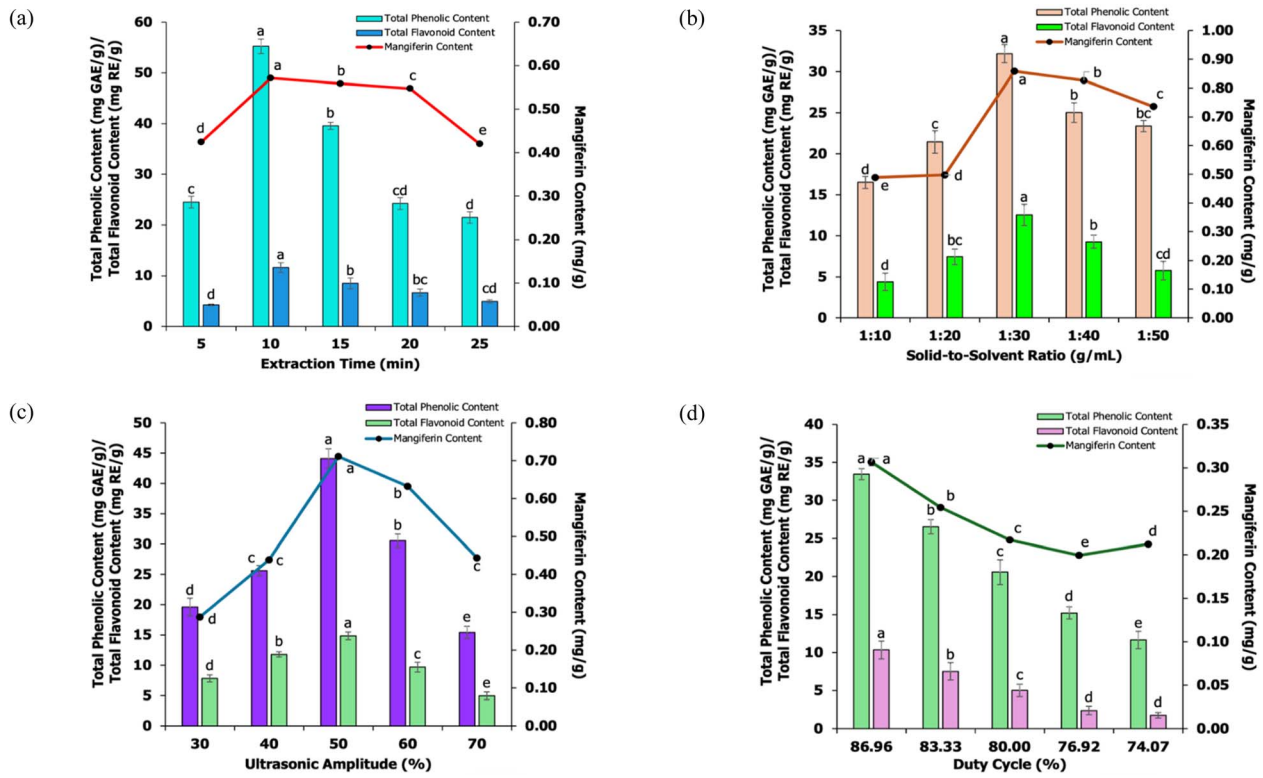

Fig. 1 Screening of extraction parameters for total phenolic content and total flavonoid content (bars) and mangiferin content (line) at different (a) extraction times, (b) solid-to-solvent ratios, (c) ultrasonic amplitudes, and (d) duty cycles. Data are presented as mean ± SD ($n = 3$), with different letters indicating significant differences ($p < 0.05$) according to one-way ANOVA and Tukey's HSD test.

solvent ratio (1 : 30 g mL^{-1}), ultrasonic amplitude (50%), and duty cycle (86.96%) were kept constant. As shown in Fig. 1(a), all three responses reached their maximum values at 10 min. The TPC increased from 24.52 ± 1.14 to 55.24 ± 1.43 mg GAE g^{-1}, TFC from 4.28 ± 0.16 to 11.63 ± 0.96 mg RE g^{-1}, and mangiferin content from 0.42 ± 0.00 to 0.57 ± 0.00 mg g^{-1} as the extraction time increased from 5 to 10 min ($p < 0.05$). These results are consistent with the study by Thakare *et al.*,[41] which reported the maximum mangiferin content at 10 min before a slight decline at longer extraction times. Although longer extraction times generally improve extraction through enhanced solvent penetration and ultrasonic cavitation, prolonged exposure may also promote degradation of bioactive compounds.[26] Accordingly, all three responses declined beyond 10 min, with the TPC decreasing to 39.60 ± 0.70, 24.52 ± 1.14, and 21.48 ± 1.12 mg GAE g^{-1}, TFC to 8.51 ± 1.09, 6.58 ± 0.32, and 4.96 ± 0.32 mg RE g^{-1}, and mangiferin content to 0.56 ± 0.00, 0.55 ± 0.00, and 0.42 ± 0.00 mg g^{-1} at 15, 20, and 25 min, respectively ($p < 0.05$). Exceeding the optimal extraction time may therefore cause degradation of bioactive compounds due to cavitation effects and oxidation caused by free radicals generated during bubble collapse.[42] Considering the cost, operating time, and energy consumption, an extraction time of 5 to 15 min was selected for further optimisation.

3.1.2 Effects of solid-to-solvent ratio on TPC, TFC, and mangiferin content. TPC, TFC, and mangiferin content of MPFE at different solid-to-solvent ratios were evaluated under fixed conditions of extraction time (15 min), ultrasonic amplitude (50%), and duty cycle (80.00%). As shown in Fig. 1(b), the TPC increased from 16.50 ± 0.73 to 21.45 ± 1.38 mg GAE g^{-1}, TFC from 4.41 ± 1.06 to 7.45 ± 0.94 mg RE g^{-1}, and mangiferin content from 0.49 ± 0.00 to 0.50 ± 0.00 mg g^{-1} as the solid-to-solvent ratio increased from 1 : 10 to 1 : 20 g mL^{-1} ($p < 0.05$). At 1 : 30 g mL^{-1}, maximum values were obtained for the TPC (32.19 ± 1.11 mg GAE g^{-1}), TFC (12.54 ± 1.30 mg RE g^{-1}), and mangiferin content (0.86 ± 0.00 mg g^{-1}), which were significantly higher than those at lower ratios ($p < 0.05$). Increasing the solid-to-solvent ratio during ultrasonic extraction enhances the process by improving contact between the solid and solvent and reducing the mixture density.[43] This allows sound waves to propagate more effectively and promotes cavitation-induced disruption of the solid matrix. Beyond 1 : 30 g mL^{-1}, the TPC decreased to 25.01 ± 1.18 mg GAE g^{-1} at 1 : 40 g mL^{-1} and 23.37 ± 0.68 mg GAE g^{-1} at 1 : 50 g mL^{-1}, with a significant reduction observed at 1 : 40 g mL^{-1} compared with 1 : 30 g mL^{-1} ($p < 0.05$), whereas the difference between 1 : 40 and 1 : 50 g mL^{-1} was not significant ($p > 0.05$). Similarly, the TFC decreased to 9.28 ± 0.79 mg RE g^{-1} at 1 : 40 g mL^{-1} and 5.78 ± 1.13 mg RE g^{-1} at 1 : 50 g mL^{-1}, with both values being significantly lower than that at 1 : 30 g mL^{-1} ($p < 0.05$), and the reduction from 1 : 40 to 1 : 50 g mL^{-1} was also significant ($p < 0.05$). Mangiferin content also declined to 0.83 ± 0.00 mg g^{-1} at 1 : 40 g mL^{-1} and 0.74 ± 0.00 mg g^{-1} at 1 : 50 g mL^{-1}, with each decrease being significant ($p < 0.05$). Wang *et al.*[44] reported that a high solid-to-liquid ratio in ultrasonic extraction generates excess bubbles, which can limit contact between polyphenols and solvent. This phenomenon also interferes with ultrasound propagation, reducing the extraction efficiency. Based on these findings, the range of solid-to-solvent ratios prescribed for CCD was set at 1 : 20 to 1 : 40 g mL^{-1}.

3.1.3 Effects of ultrasonic amplitude on TPC, TFC, and mangiferin content. The effects of ultrasonic amplitude on TPC, TFC, and mangiferin content were evaluated under fixed conditions of extraction time (15 min), solid-to-solvent ratio (1 : 30 g mL^{-1}), and duty cycle (86.96%). As shown in Fig. 1(c), the TPC increased significantly from 19.62 ± 1.46 mg GAE g^{-1} at 30% to 44.10 ± 1.60 mg GAE g^{-1} at 50% ultrasonic amplitude ($p < 0.05$), before decreasing significantly to 30.56 ± 1.12 mg GAE g^{-1} at 60% and 15.43 ± 0.99 mg GAE g^{-1} at 70% ($p < 0.05$). A similar pattern was observed for the TFC, which increased significantly from 7.81 ± 0.59 mg RE g^{-1} at 30% to 14.83 ± 0.62 mg RE g^{-1} at 50%, followed by a significant decrease to 9.69 ± 0.81 mg RE g^{-1} at 60% and 4.95 ± 0.61 mg RE g^{-1} at 70% ($p < 0.05$). Mangiferin content also reached its maximum at 50% ultrasonic amplitude (0.71 ± 0.00 mg g^{-1}), which was significantly higher than the values recorded at 30% (0.29 ± 0.00 mg g^{-1}), 40% (0.44 ± 0.00 mg g^{-1}), 60% (0.63 ± 0.00 mg g^{-1}), and 70% (0.44 ± 0.00 mg g^{-1}) ($p < 0.05$). The value at 60% was also significantly higher than those at 30%, 40%, and 70% ($p < 0.05$), whereas the values at 30%, 40%, and 70% were not significantly different from one another ($p > 0.05$). Pattnaik *et al.*[45] reported that phenolic compound recovery increases with ultrasonic amplitude due to improved contact between the sample and solvent, which enhances both mechanical and cavitation effects. Nonetheless, excessively high amplitudes may reduce extraction efficiency because the excessive number of bubbles collides more frequently, leading to non-spherical collapses that weaken implosion forces and diminish the overall effect.[28] Considering these findings, the lower, middle, and upper levels of ultrasonic amplitude selected for the optimisation design were 40%, 50%, and 60%.

3.1.4 Effects of duty cycle on TPC, TFC, and mangiferin content. The effects of duty cycle on TPC, TFC, and mangiferin content of MPFE were evaluated under fixed conditions of extraction time (15 min), solid-to-solvent ratio (1 : 30 g mL^{-1}), and ultrasonic amplitude (50%). As shown in Fig. 1(d), the maximum TPC (33.46 ± 0.73 mg GAE g^{-1}), TFC (10.34 ± 1.18 mg RE g^{-1}), and mangiferin content (0.31 ± 0.00 mg g^{-1}) were obtained at a duty cycle of 86.96% ($p < 0.05$). Pulse mode enhances cavitation efficiency and provides stable temperature control, thereby preventing degradation of phytochemicals.[46] The duty cycle of an ultrasound system represents the operational cycle that allows it to function in pulsed mode, alternating between on and off phases.[47] The pulsed phase has been shown to provide superior results compared with continuous mode.[48] Moreover, pulse mode ultrasonication in natural product extraction extends the life of the transducer and reduces unnecessary energy losses.[49] Lanjekar *et al.*[25] reported an optimum duty cycle of 60% (6 s on and 4 s off) for waste *Mangifera indica* (mango) peel extract, which produced the highest values of TPC and TFC, with yields declining between 60% and 100%. In the present study, all three responses decreased as the duty cycle decreased from 86.96% to 74.07%. The TPC decreased significantly from 33.46 ± 0.73 mg GAE g^{-1}

at 86.96% to 26.53 ± 0.92, 20.49 ± 1.91, 15.12 ± 0.70, and 11.66 ± 1.14 mg GAE g^{-1} at 83.33%, 80.00%, 76.92%, and 74.07%, respectively ($p < 0.05$). The TFC also decreased significantly from 10.34 ± 1.18 mg RE g^{-1} at 86.96% to 7.52 ± 1.13, 5.02 ± 0.80, 2.40 ± 0.56, and 1.76 ± 0.36 mg RE g^{-1}, respectively ($p < 0.05$), although the difference between 76.92% and 74.07% was not significant ($p > 0.05$). Mangiferin content decreased significantly from 0.31 ± 0.00 mg g^{-1} at 86.96% to 0.25 ± 0.00, 0.22 ± 0.00, 0.20 ± 0.00, and 0.21 ± 0.00 mg g^{-1} at 83.33%, 80.00%, 76.92%, and 74.07%, respectively ($p < 0.05$). These reductions may be attributed to excess heat generated by prolonged exposure of the solvent to acoustic waves. In addition, uncontrolled cavitation and excessive mechanical stress during extraction may degrade phenolic compounds.[23] For this reason, the duty cycle of 86.96% was maintained in the CCD process.

3.2 Optimisation of extraction parameters using CCD

The optimisation study focused on three factors: extraction time (A), solid-to-solvent ratio (B), and ultrasonic amplitude (C), while keeping the duty cycle constant at 86.96%. These parameters were selected to identify the most significant factors influencing the responses, to establish the most suitable model, to explain their effects on TPC, TFC, and mangiferin content, and to verify the accuracy of the optimisation process.

3.2.1 Model fitting for TPC, TFC, and mangiferin content. All data were fitted to several models, including linear, two-factor interaction (2FI), quadratic, and cubic models, to statistically evaluate model adequacy. As shown in Table 3, the quadratic model was identified as the most appropriate for the three responses due to its higher significance of fit, lower SD (1.18 for TPC, 0.50 for TFC, and 0.03 for mangiferin content), and lower predicted residual error sum of squares (PRESS) values (63.76 for TPC, 10.81 for TFC, and 0.04 for mangiferin content) compared with the other models. Thus, the quadratic model was selected to describe the relationship between the input and response variables.

Khoshraftar *et al.*[50] highlighted the significance of regression model, lack of fit, R^2, and CV as key criteria for evaluating model adequacy and validity. As shown in Table 4, the R^2 values for TPC (0.9944), TFC (0.9912), and mangiferin content (0.9909) were close to one, indicating minimal fitting errors and confirming the robustness of the model.[51] The adjusted R^2 values, which eliminate unnecessary terms, were also close to the R^2 values, suggesting high significance of the quadratic model. Predicted R^2 values were in reasonable agreement with adjusted R^2 values for TPC, TFC, and mangiferin content, as their differences were less than 0.2, which indicates satisfactory model adequacy.[52] The CV values of TPC (3.31%), TFC (4.85%), and mangiferin content (6.64%) were below 10%, indicating that the experimental results were precise and reliable.[53] Adequate precision ratios for TPC (36.0761), TFC (28.5614), and mangiferin content (31.8071) were greater than 4, indicating excellent signal-to-noise ratios and confirming that the models can be used reliably to navigate the design space.[50]

ANOVA was employed to analyse the statistical interactions between factors and response variables in the model.[54] Multiple regression results and the significance of regression coefficients are presented in Table 5. Khoshraftar *et al.*[50] indicated that

Table 3 Model fitting summary for total phenolic content, total flavonoid content, and mangiferin content

Source	SD	R^2	Adjusted R^2	Predicted R^2	PRESS	
Total phenolic content						
Linear	10.83	0.1242	−0.0779	−0.1563	2012.11	
2FI	11.84	0.1947	−0.2884	−0.5760	2742.54	
Quadratic	1.18	0.9944	0.9872	0.9634	63.76	Suggested
Cubic	1.42	0.9965	0.9816	0.4862	894.03	Aliased
Total flavonoid content						
Linear	3.46	0.2086	0.0259	−0.0603	208.98	
2FI	3.74	0.2886	−0.1383	−0.4331	282.45	
Quadratic	0.50	0.9912	0.9798	0.9451	10.81	Suggested
Cubic	0.48	0.9966	0.9817	0.7745	44.44	Aliased
Mangiferin content						
Linear	0.19	0.2187	0.0384	−0.2960	0.76	
2FI	0.19	0.3704	−0.0074	−0.3145	0.77	
Quadratic	0.03	0.9909	0.9793	0.9386	0.04	Suggested
Cubic	0.02	0.9974	0.9860	0.7408	0.15	Aliased

Table 4 Fit statistics for total phenolic content, total flavonoid content, and mangiferin content

Response	Mean	SD	CV (%)	R^2	Adjusted R^2	Predicted R^2	Adequate precision
Total phenolic content	35.75	1.18	3.31	0.9944	0.9872	0.9634	36.0761
Total flavonoid content	10.28	0.4986	4.85	0.9912	0.9798	0.9451	28.5614
Mangiferin content	0.4153	0.0276	6.64	0.9909	0.9793	0.9386	31.8071

a satisfactory model fit is achieved when the overall model is significant ($p < 0.05$), while the lack of fit is not significant ($p > 0.05$). In this study, the models for TPC, TFC, and mangiferin content were highly significant ($p < 0.0001$). The lack of fit *F*-values for TPC (1.58), TFC (1.05), and mangiferin content (2.05) were not significant relative to pure error ($p > 0.05$). The model *F*-values for TPC (137.58), TFC (87.30), and mangiferin content (85.13) were highly significant ($p < 0.0001$), confirming the robustness of the models. For TPC, term *B* was significant ($p < 0.05$), while terms *A*, *BC*, A^2, B^2, and C^2 were highly significant ($p < 0.0001$). For TFC, terms *C*, *AC*, and *BC* were significant ($p < 0.05$), while terms *A*, *B*, A^2, B^2, and C^2 were highly significant ($p < 0.0001$). For mangiferin content, terms *A*, *AC*, and B^2 were significant ($p < 0.05$), while terms *C*, *BC*, A^2, and C^2 were highly significant ($p < 0.0001$).

The statistical results confirm that the models were adequate for predicting TPC, TFC, and mangiferin content within the studied ranges of design parameters. With $p < 0.0001$, the models were highly reliable, and the significant terms demonstrated measurable effects on the responses. Multiple regression analysis produced eqn (7)–(9), which described the relationships between the factors and the response variables of TPC, TFC, and mangiferin content, respectively.

$$\text{Total phenolic content} = 55.22 + 3.73A - 1.37B + 3.86BC - 8.30A^2 - 8.28B^2 - 7.65C^2 \quad (7)$$

$$\text{Total flavonoid content} = 16.40 + 1.23A - 1.15B + 0.4285C + 0.4327AC + 1.29BC - 2.47A^2 - 2.40B^2 - 2.76C^2 \quad (8)$$

Table 5 ANOVA summary for total phenolic content, total flavonoid content, and mangiferin content

Source	Sum of squares	d*f*	Mean square	*F*-value	*P*-value	
Total phenolic content						
Model	1730.37	9	192.26	137.58	<0.0001	Significant
A	190.06	1	190.06	136.01	<0.0001	
B	25.73	1	25.73	18.41	0.0036	
C	0.3435	1	0.3435	0.2458	0.6352	
AB	0.0000	1	0.0000	0.0000	0.9954	
AC	3.34	1	3.34	2.39	0.1662	
BC	119.38	1	119.38	85.43	<0.0001	
A^2	776.93	1	776.93	555.97	<0.0001	
B^2	773.69	1	773.69	553.65	<0.0001	
C^2	659.08	1	659.08	471.64	<0.0001	
Residual	9.78	7	1.40			
Lack of fit	7.80	5	1.56	1.58	0.4320	Not significant
Pure error	1.98	2	0.9904			
Total flavonoid content						
Model	195.35	9	21.71	87.30	<0.0001	Significant
A	20.61	1	20.61	82.89	<0.0001	
B	17.99	1	17.99	72.34	<0.0001	
C	2.51	1	2.51	10.09	0.0156	
AB	1.04	1	1.04	4.16	0.0806	
AC	1.50	1	1.50	6.03	0.0438	
BC	13.24	1	13.24	53.25	0.0002	
A^2	68.76	1	68.76	276.53	<0.0001	
B^2	64.81	1	64.81	260.65	<0.0001	
C^2	85.69	1	85.69	344.65	<0.0001	
Residual	1.74	7	0.2486			
Lack of fit	1.26	5	0.2520	1.05	0.5542	Not significant
Pure error	0.4807	2	0.2403			
Mangiferin content						
Model	0.5819	9	0.0647	85.13	<0.0001	Significant
A	0.0163	1	0.0163	21.50	0.0024	
B	6.673×10^{-6}	1	6.673×10^{-6}	0.0088	0.9279	
C	0.1121	1	0.1121	147.59	<0.0001	
AB	0.0024	1	0.0024	3.23	0.1155	
AC	0.0288	1	0.0288	37.92	0.0055	
BC	0.0578	1	0.0578	76.10	<0.0001	
A^2	0.0513	1	0.0513	67.57	<0.0001	
B^2	0.0052	1	0.0052	6.87	0.0344	
C^2	0.3465	1	0.3465	456.17	<0.0001	
Residual	0.0053	7	0.0008			
Lack of fit	0.0044	5	0.0009	2.05	0.3591	Not significant
Pure error	0.0009	2	0.0004			

$$\text{Mangiferin content} = 0.6276 + 0.0346A + 0.0906C + 0.0600AC - 0.0850BC - 0.0675A^2 - 0.0215B^2 - 0.1753C^2 \quad (9)$$

The normal probability plots of residuals for TPC, TFC, and mangiferin content in Fig. 2(a)–(c) showed that the residuals largely aligned with the theoretical red line, confirming the adequacy of the models.[55] Predicted *versus* actual values in Fig. 2(d)–(f) demonstrated strong agreement, indicating that the models could reliably predict the three responses. Residuals *versus* run plots in Fig. 2(g)–(i) showed that all data points were within the critical range of −4.81963 to +4.81963, confirming that the models were significant and acceptable, with no outliers detected.

3.2.2 Perturbation analysis for TPC, TFC, and mangiferin content. The perturbation plots in Fig. 3 illustrate the effects of individual factors on the response variables (TPC, TFC, and mangiferin content) of the MPFE by varying one factor at a time while keeping the others constant at a specific point in the design space.[56] As shown in Fig. 3(a), the perturbation plot for TPC indicated that extraction time (*A*) exerted the strongest effect, followed by solid-to-solvent ratio (*B*), whereas ultrasonic amplitude (*C*) had a relatively smaller influence. Similarly, Fig. 3(b) shows that extraction time (*A*) and solid-to-solvent ratio (*B*) were the most influential factors for TFC, as indicated by their steeper curvature relative to ultrasonic amplitude (*C*). This observation is consistent with the explanation that a greater curvature reflects the higher sensitivity of the response to changes in a factor, whereas a lower curvature indicates a weaker influence.[57] For mangiferin content, the perturbation plot in Fig. 3(c) showed that ultrasonic amplitude (*C*) exerted the strongest effect, as indicated by the pronounced parabolic curvature of the response plot. The curve also suggests that the highest mangiferin content was achieved near the central region of the design space, with a slight shift towards the positive coded level of ultrasonic amplitude.

3.2.3 Effects of extraction parameters on TPC. Three-dimensional response surface and contour plots of RSM were generated to visualise the effects of extraction time (*A*), solid-to-solvent ratio (*B*), and ultrasonic amplitude (*C*) on TPC, as presented in Fig. 4(a)–(c), respectively. The three-dimensional response surface plots and corresponding contour plots were generated by varying two parameters while keeping the third constant in order to evaluate their combined effects on the response. Overall, both plot types indicate that TPC increased towards the central region of the design space and declined at lower or higher factor levels. For the interaction between the extraction time and solid-to-solvent ratio, the optimum region was observed at approximately 9–13 min and 1 : 25–1 : 35 g mL^{-1}, respectively, at a constant ultrasonic amplitude of 50%.

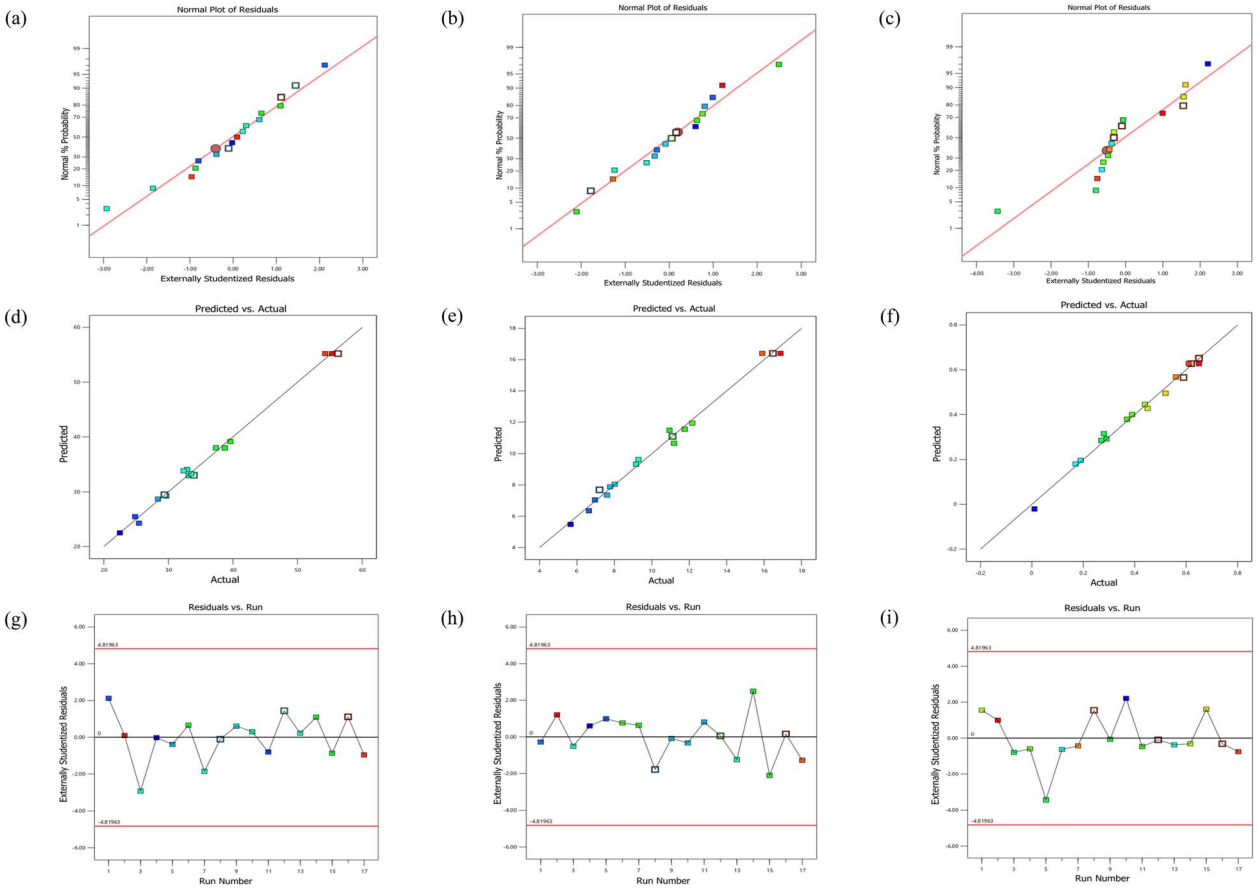

Fig. 2 Statistical analysis related to MPFE: (a–c) normal plots of residuals for total phenolic content, total flavonoid content, and mangiferin content, (d–f) relationships between predicted and actual values, and (g–i) residuals *versus* run of experiments.

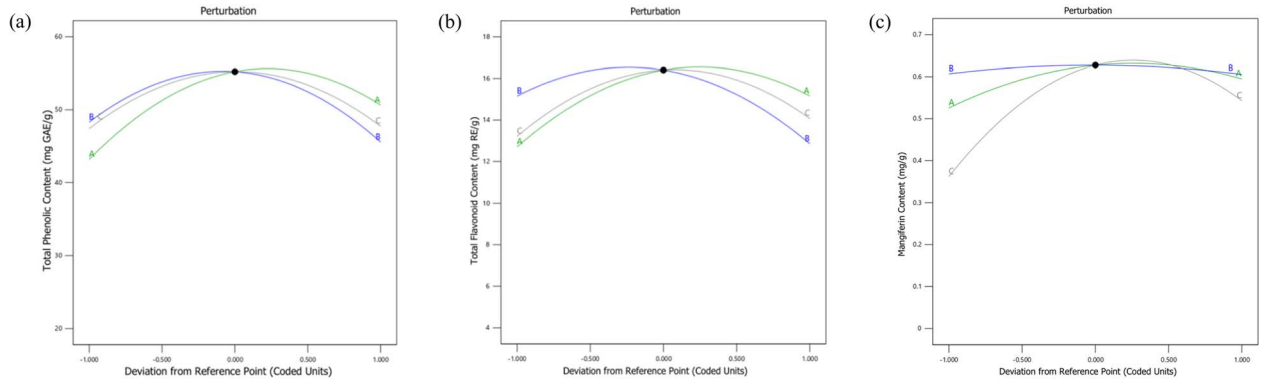

Fig. 3 Perturbation plots for (a) total phenolic content, (b) total flavonoid content, and (c) mangiferin content.

For the interaction between the extraction time and ultrasonic amplitude, the optimum region occurred at approximately 9–13 min and 45–55%, respectively, at a constant solid-to-solvent ratio of 1 : 30 g mL^{-1}. Similarly, for the interaction between the solid-to-solvent ratio and ultrasonic amplitude, the highest TPC was achieved at approximately 1 : 25–1 : 35 g mL^{-1} and 45–55%, respectively, at a constant extraction time of 10 min.[58] By contrast, terms *C*, *AB*, and *AC* were not significant ($p > 0.05$). Anaya-Esparza *et al.*[59] similarly reported that higher solvent ratios improve solvent penetration into plant tissues and facilitate compound extraction, while Lima *et al.*[60] found that ultrasonic amplitude enhances extraction only up to an optimum level, beyond which the extraction efficiency declines. These observations are consistent with the ANOVA results, in which term *B* was significant ($p < 0.05$), while terms *A*, *BC*, A^2, B^2, and C^2 were highly significant ($p < 0.0001$).

3.2.4 Effects of extraction parameters on TFC. Three-dimensional response surface and contour plots of RSM were generated to visualise the effects of extraction time (*A*), solid-to-solvent ratio (*B*), and ultrasonic amplitude (*C*) on TFC, as presented in Fig. 5(a)–(c), respectively. The plots were generated by varying two parameters while keeping the third constant in order to evaluate their combined effects on the response. Overall, the response surfaces and contour plots indicate that TFC increased towards the central region of the design space and declined at lower or higher factor levels. For the interaction between the extraction time and solid-to-solvent ratio, the optimum region was observed at approximately 9–13 min and 1 : 25–1 : 35 g mL^{-1}, respectively, at a constant ultrasonic amplitude of 50%. However, TFC decreased at higher solid-to-solvent ratios despite the longer extraction time, which may be attributed to prolonged extraction conditions that promote flavonoid degradation.[61] For the interaction between the extraction time and ultrasonic amplitude, the optimum region occurred at approximately 9–13 min and 45–55%, respectively, at a constant solid-to-solvent ratio of 1 : 30 g mL^{-1}. TFC declined when the ultrasonic amplitude exceeded approximately 55%, even within the favourable extraction time range, which may reflect excessive cavitation effects that destabilise flavonoid compounds. As explained by Garcia-Larez *et al.*,[62] higher ultrasonic amplitudes can generate intense cavitation that disrupts molecular structures and increases susceptibility to flavonoid degradation. For the interaction between the solid-to-solvent ratio and ultrasonic amplitude, the optimum region was observed at approximately 1 : 25–1 : 35 g mL^{-1} and 45–55%, respectively, at a constant extraction time of 10 min. Mehganathan *et al.*[63] reported that greater extraction efficiency can be achieved when cavitation disrupts plant cell walls and an increased solvent volume enhances the concentration gradient, thereby accelerating flavonoid mass transfer into the solvent. These observations are consistent with the ANOVA results, in which term *AB* was not significant ($p > 0.05$), term *AC* was significant ($p < 0.05$), and term *BC* was highly significant ($p = 0.0002$). Additionally, term *C* was significant ($p < 0.05$), while terms *A*, *B*, A^2, B^2, and C^2 were highly significant ($p < 0.0001$).

3.2.5 Effects of extraction parameters on mangiferin content. Three-dimensional response surface and contour plots of RSM were generated to visualise the effects of extraction time (*A*), solid-to-solvent ratio (*B*), and ultrasonic amplitude (*C*) on mangiferin content, as presented in Fig. 6(a)–(c), respectively. The plots were generated by varying two parameters while keeping the third constant in order to evaluate their combined effects on the response. Overall, the response surfaces and contour plots indicate that mangiferin content increased towards the central region of the design space, although the influence of each factor differed. For the interaction between the extraction time and solid-to-solvent ratio, mangiferin content remained relatively unchanged across the solid-to-solvent ratio range at shorter extraction times, and it increased as the extraction time approached the middle region of the design space. The optimum region was observed at approximately 7–13 min and 1 : 25–1 : 35 g mL^{-1}, respectively, at a constant ultrasonic amplitude of 50%. However, mangiferin content declined when the extraction time exceeded the optimum level. Xue *et al.*[64] reported a similar trend, in which compound recovery increased with the solid-to-solvent ratio up to an optimum level due to improved contact area and a steeper concentration gradient that facilitated diffusion into the solvent. For the interaction between the extraction time and ultrasonic amplitude, the optimum region occurred at approximately 7–13 min and 45–55%, respectively, at a constant solid-to-solvent ratio of 1 : 30 g mL^{-1}. Increased β-carotene extraction from cashew apple fruit was similarly observed at optimum extraction conditions, where sufficient ultrasonic intensity

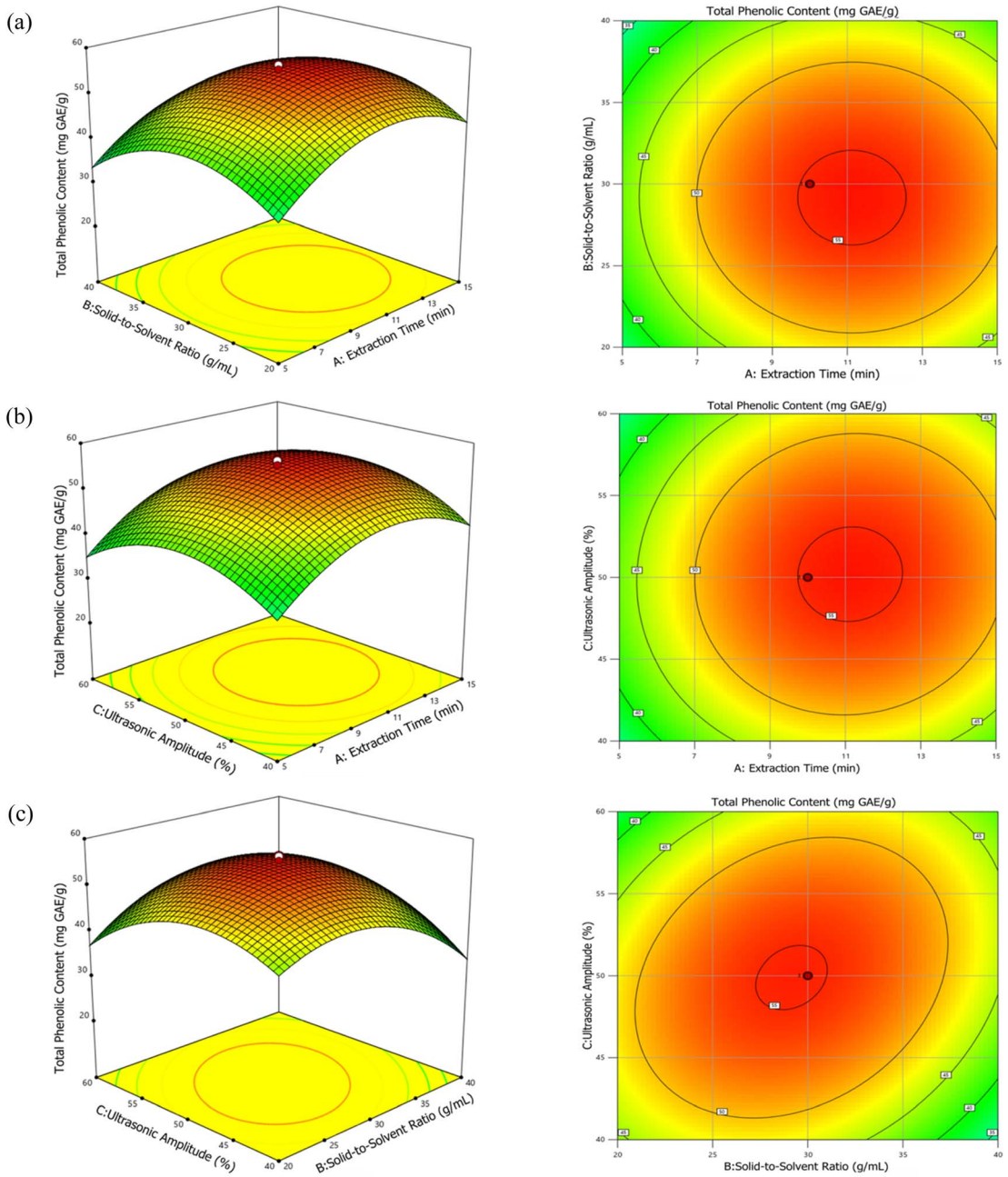

Fig. 4 3D surface and contour plots of total phenolic content of MPFE for (a) extraction time (*A*) *versus* solid-to-solvent ratio (*B*) at constant ultrasonic amplitude (50%), (b) extraction time (*A*) *versus* ultrasonic amplitude (*C*) at constant solid-to-solvent ratio (1 : 30 g mL^{-1}), and (c) solid-to-solvent ratio (*B*) *versus* ultrasonic amplitude (*C*) at constant extraction time (10 min).

promoted cell wall disruption and enhanced compound release.[65] For the interaction between solid-to-solvent ratio and ultrasonic amplitude, the highest mangiferin content was observed when the solid-to-solvent ratio ranged from approximately 1 : 25 to 1 : 35 g mL^{-1} and the ultrasonic amplitude from 45 to 55% at a constant extraction time of 10 min. Moldovan *et al.*[66] likewise reported that a moderate ultrasonic amplitude produced a higher recovery of phenolic and flavonoid compounds from shallot (*Allium ascalonicum*) peel than a higher intensity, at which degradation became more likely. These observations are consistent with the ANOVA results, in which terms *A*, *AC*, and B^2 were significant ($p < 0.05$), while terms *C*, *BC*, A^2, and C^2 were highly significant ($p < 0.0001$). By contrast, terms *B* and *AB* were not significant ($p > 0.05$).

3.2.6 Desirability and verification of the predictive model. The optimal extraction conditions for maximising TPC, TFC, and mangiferin content were obtained from the ramp plots in Fig. 7(a). The predicted optimum conditions were an extraction time of 11.33 min, a solid-to-solvent ratio of 1 : 28.52 g mL^{-1}, and an ultrasonic amplitude of 51.41%. Under these conditions, the predicted responses were 55.46 mg GAE g^{-1} for TPC, 16.68 mg RE g^{-1} for TFC, and 0.65 mg g^{-1} for mangiferin

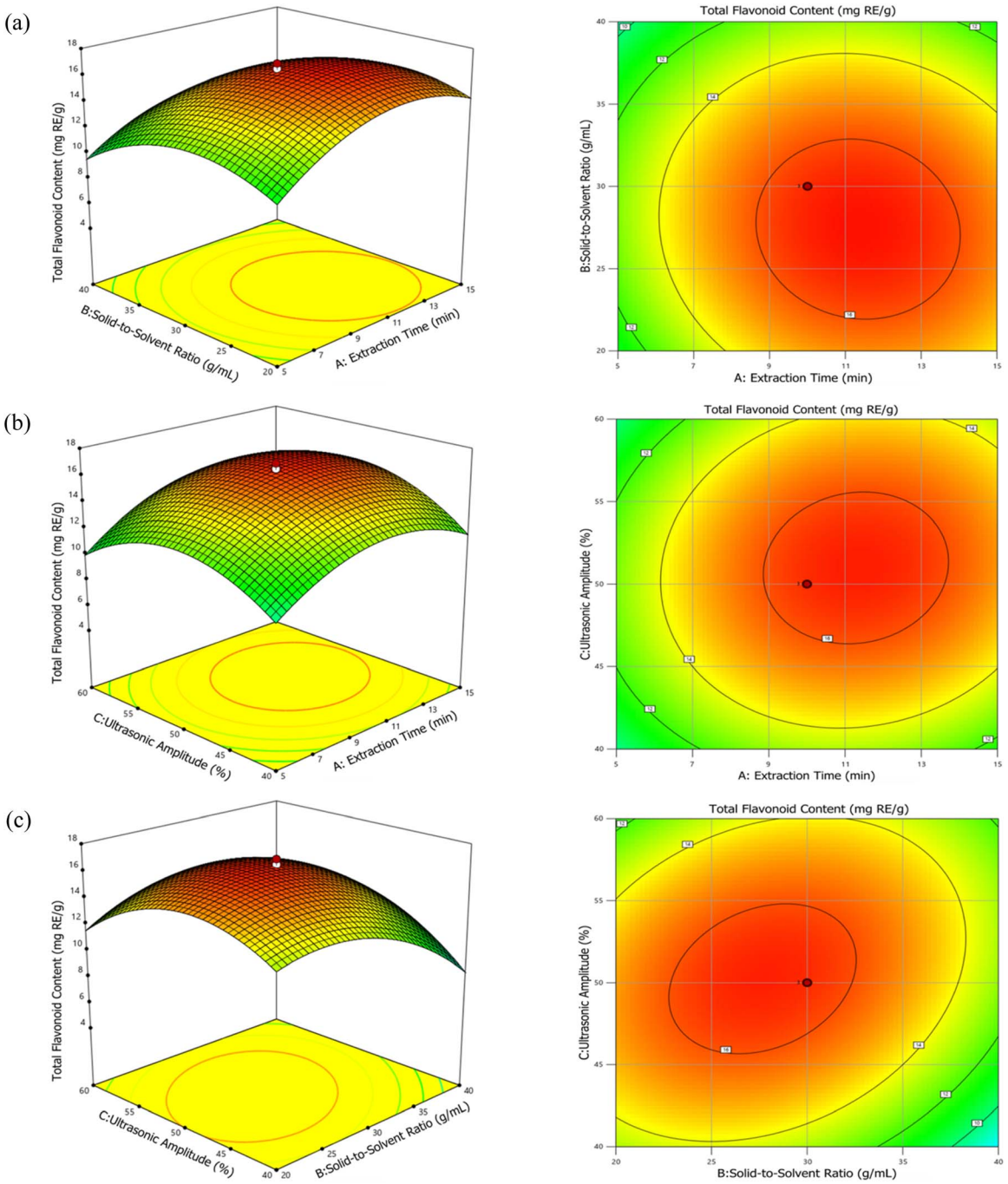

Fig. 5 3D surface and contour plots of total flavonoid content of MPFE for (a) extraction time (*A*) *versus* solid-to-solvent ratio (*B*) at constant ultrasonic amplitude (50%), (b) extraction time (*A*) *versus* ultrasonic amplitude (*C*) at constant solid-to-solvent ratio (1 : 30 g mL^{-1}), and (c) solid-to-solvent ratio (*B*) *versus* ultrasonic amplitude (*C*) at constant extraction time (10 min).

content, with an overall desirability of 0.984. This indicates a high degree of suitability of the selected factor combination for achieving the target responses.[57] Fig. 7(b) presents the desirability values for each factor and response variable of MPFE. In this study, numerical optimisation based on the desirability function was applied to identify the most suitable extraction conditions. Becze *et al.*[67] reported that model validity is supported when actual values are in close agreement with predicted values. As shown in Table 6, the actual and predicted values were 53.02 ± 1.57 and 55.46 mg GAE g^{-1} for TPC, 17.26 ± 1.13 and 16.68 mg RE g^{-1} for TFC, and 0.66 ± 0.01 and 0.65 mg g^{-1} for mangiferin content, corresponding to percentage errors of 4.60%, 3.36%, and 1.52%, respectively.

3.3 Antioxidant and antidiabetic activity of the optimised MPFE

Fig. 8(a) and (b) present the concentration–response curves used for IC_{50} determination of DPPH radical scavenging and α-

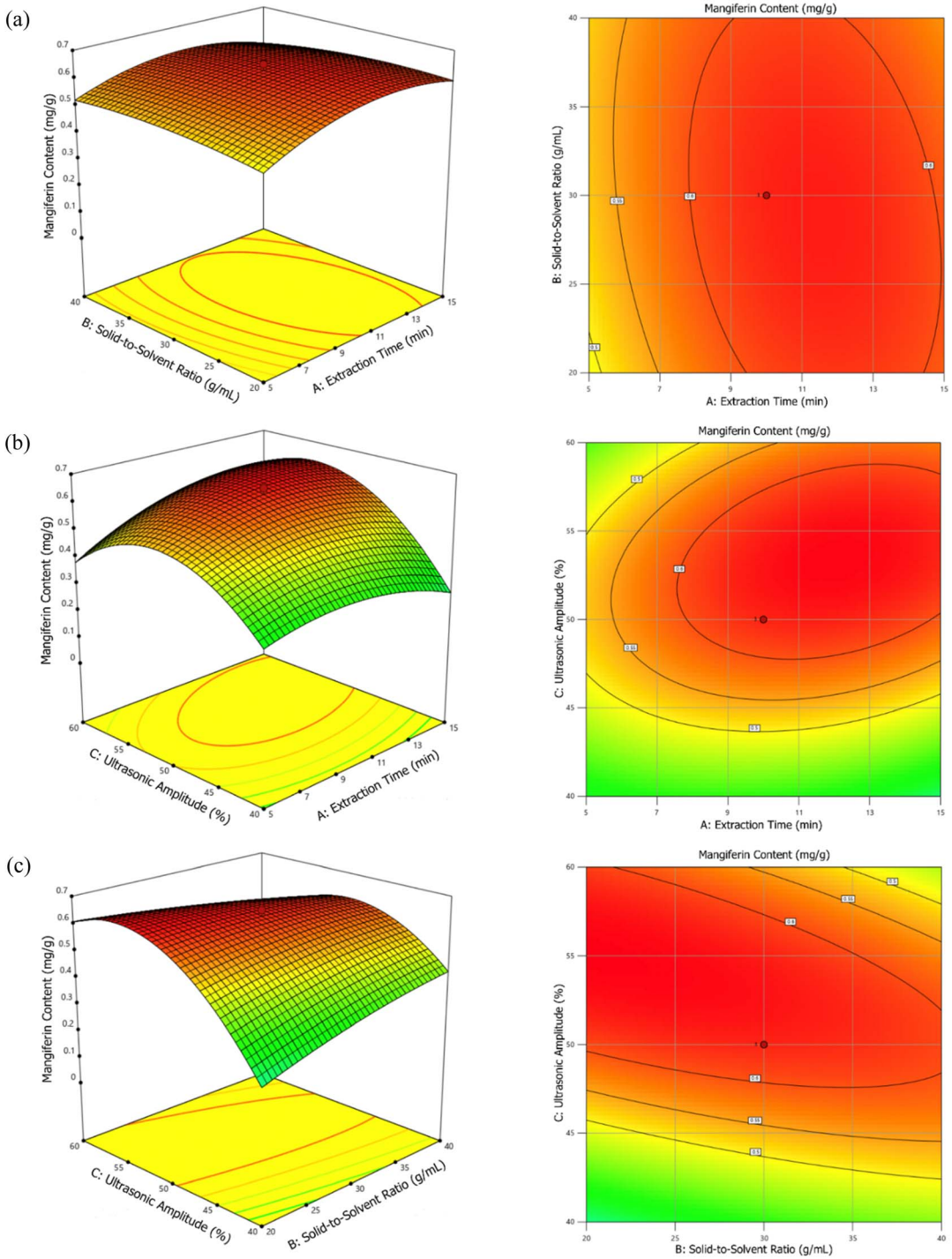

Fig. 6 3D surface and contour plots of mangiferin content of MPFE for (a) extraction time (*A*) *versus* solid-to-solvent ratio (*B*) at constant ultrasonic amplitude (50%), (b) extraction time (*A*) *versus* ultrasonic amplitude (*C*) at constant solid-to-solvent ratio (1 : 30 g mL^{-1}), and (c) solid-to-solvent ratio (*B*) *versus* ultrasonic amplitude (*C*) at constant extraction time (10 min).

glucosidase inhibitory activities of the optimised MPFE. For DPPH activity, the concentrations tested were ascorbic acid (5–100 μg mL^{-1}), mangiferin (5–100 μg mL^{-1}), and MPFE (5–1000 μg mL^{-1}). For α-glucosidase activity, the concentrations tested were acarbose (5–25 μg mL^{-1}), mangiferin (5–25 μg mL^{-1}), and MPFE (5–250 μg mL^{-1}). IC_{50} is defined as the concentration of a sample required to inhibit 50% of activity.[68] The observed antioxidant and antidiabetic activities of MPFE may be attributed to the presence of phytochemical constituents, including phenolic and flavonoid compounds, together with mangiferin.

As shown in Fig. 9(a), the IC_{50} value for DPPH inhibition of MPFE (117.58 ± 2.19 μg mL^{-1}) was significantly higher than

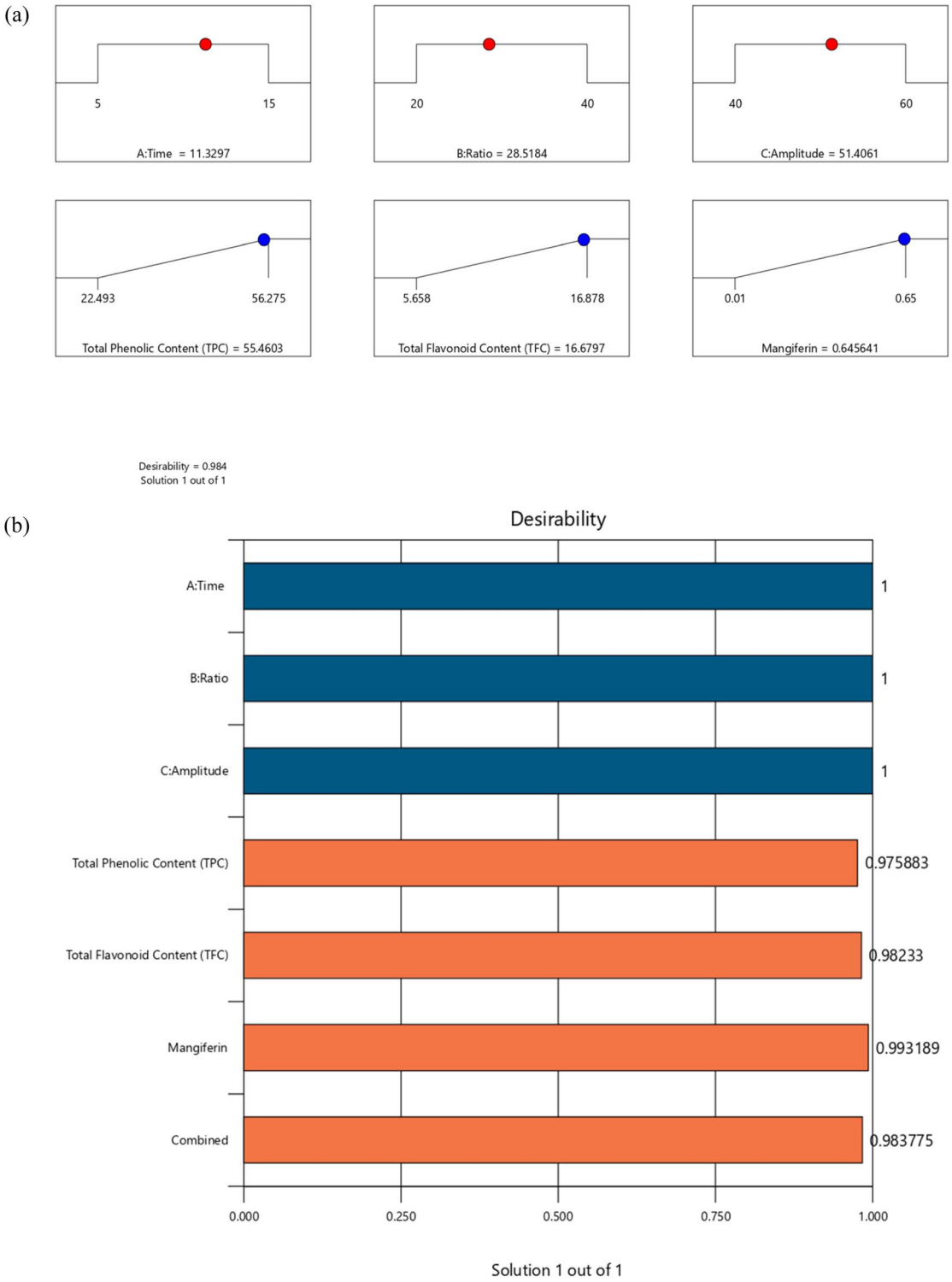

Fig. 7 Desirability analysis for optimisation of total phenolic content, total flavonoid content, and mangiferin content: (a) ramp plots and (b) bar graph.

that of mangiferin (5.19 ± 0.27 μg mL^{-1}) and ascorbic acid (5.84 ± 0.29 μg mL^{-1}), indicating a lower antioxidant potency than the positive controls. This aligns with the findings of Yehia and Altwaim,[69] who reported that mangiferin from *M. indica* leaves exhibited DPPH radical scavenging activity with an IC_{50} of 17.6 μg mL^{-1}, compared with 11.9 μg mL^{-1} for vitamin C. These results support the strong antioxidant potential of mangiferin, which may be related to its phenolic structure and hydrogen-donating capacity. For α-glucosidase inhibition, Fig. 9(b) shows IC_{50} values of 90.54 ± 1.60 μg mL^{-1} for MPFE, 1.87 ± 0.19

Table 6 Predicted and actual response values under optimised MPFE extraction conditions

Factors			
	Extraction time (min)	11.33	
	Solid-to-solvent ratio (g mL^{-1})	1 : 28.52	
	Ultrasonic amplitude (%)	51.41	
Responses	Total phenolic content (mg GAE g^{-1})	Predicted	55.46
		Actual	53.02 ± 1.57
		Error (%)	4.60
	Total flavonoid content (mg RE g^{-1})	Predicted	16.68
		Actual	17.26 ± 1.13
		Error (%)	3.36
	Mangiferin content (mg g^{-1})	Predicted	0.65
		Actual	0.66 ± 0.01
		Error (%)	1.52

μg mL^{-1} for mangiferin, and 9.48 ± 0.44 μg mL^{-1} for acarbose. These findings are consistent with the study by Sekar *et al.*,[70] which reported IC_{50} values of 112.80 μg mL^{-1} for the ripe *M. indica* fruit pulp extract, 36.84 μg mL^{-1} for mangiferin, and 21.33 μg mL^{-1} for acarbose. The markedly lower IC_{50} value of mangiferin compared with MPFE and acarbose indicates stronger α-glucosidase inhibitory activity under the conditions tested. Overall, lower IC_{50} values indicate that smaller

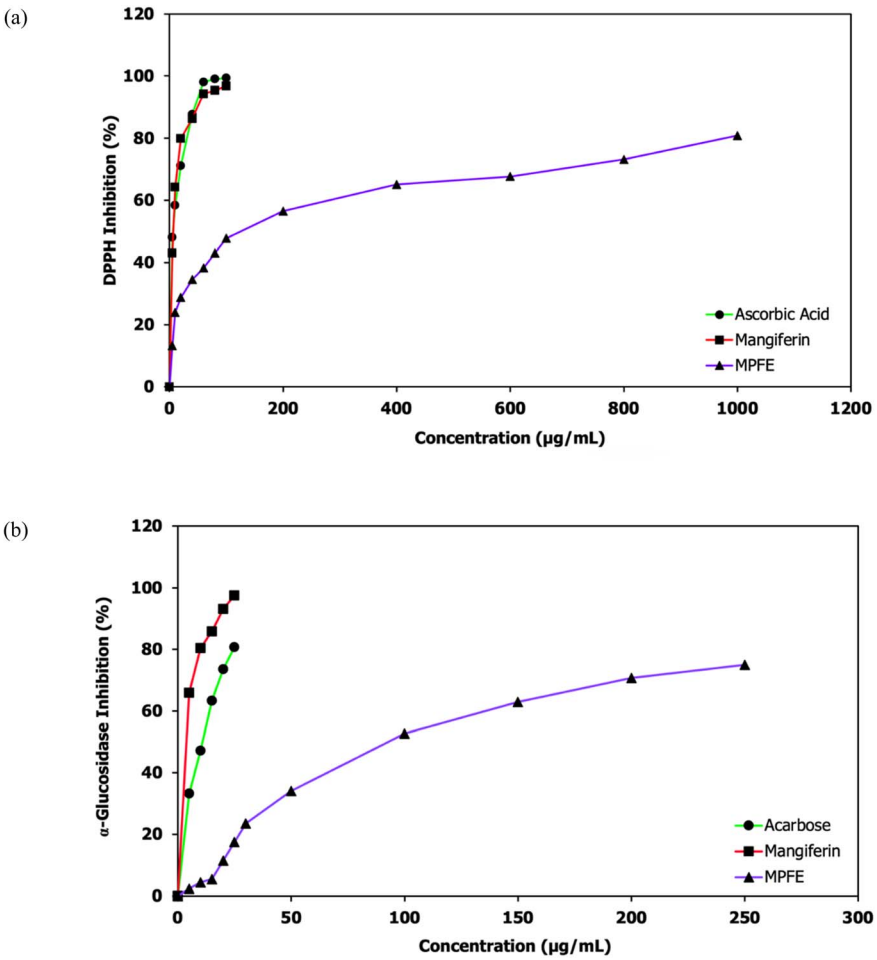

Fig. 8 (a) DPPH and (b) α-glucosidase inhibition, comparing ascorbic acid (for DPPH) and acarbose (for α-glucosidase) with mangiferin and optimised MPFE. Data are presented as mean ± SD ($n = 3$), with different letters indicating significant differences ($p < 0.05$) according to one-way ANOVA and Tukey's HSD test.

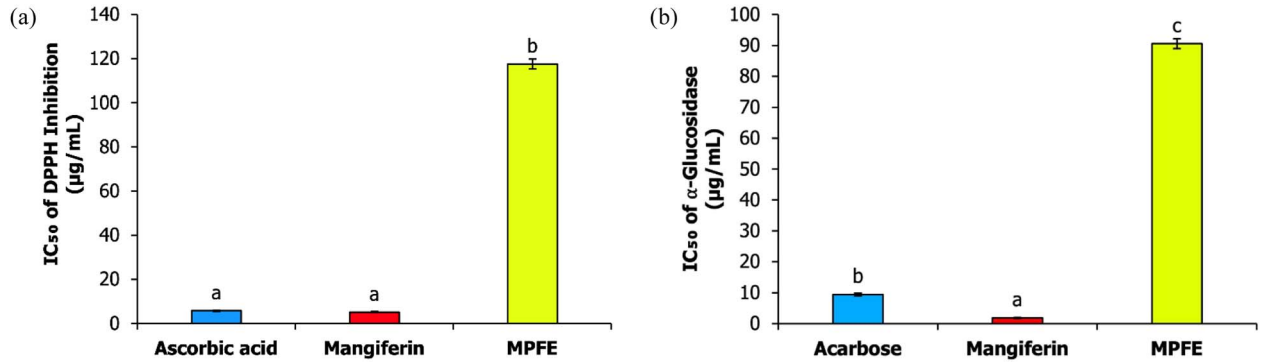

Fig. 9 IC_{50} values of (a) DPPH and (b) α-glucosidase inhibition of optimised MPFE, mangiferin, and positive controls (ascorbic acid and acarbose, respectively). Data are presented as mean ± SD ($n = 3$), with different letters indicating significant differences ($p < 0.05$) according to one-way ANOVA and Tukey's HSD test.

concentrations are required to achieve antioxidant and antidiabetic effects.

3.4 Molecular docking of α-glucosidase on antidiabetic activity of the optimised MPFE

In silico docking simulations were conducted to validate the *in vitro* enzymatic inhibitory results by evaluating docking scores, binding affinity, and molecular interactions between ligands and the target protein.[71] α-Glucosidase is a digestive enzyme responsible for hydrolysing glycosidic bonds in disaccharides and oligosaccharides, producing monosaccharides that are readily absorbed into blood vessels.[72] Acarbose, a well-known α-glucosidase inhibitor, is widely prescribed as a synthetic drug to reduce postprandial blood glucose levels, although it is associated with side effects including weight gain, hypersensitivity reactions, abdominal pain, diarrhoea, and hepatotoxicity.[73] Both ligands, mangiferin and acarbose, were docked to the α-glucosidase protein (PDB ID: 5NN8). The Vina docking scores presented in Table 7 revealed that mangiferin (−8.0 kcal mol^{-1}) exhibited stronger binding affinity at the identified binding pockets than acarbose (−7.3 kcal mol^{-1}). These findings are consistent with Yakoubi,[74] who explained that more negative AutoDock Vina scores indicate stronger ligand–protein interactions. Notably, mangiferin formed a greater number of hydrogen bond-related interactions than acarbose. Chu *et al.*[75] also reported that mangiferin was approximately five times more effective than acarbose due to its xanthone backbone, which enables multiple stable interactions during α-glucosidase inhibition.

As shown in Fig. 10, mangiferin formed twelve interaction bonds, including conventional hydrogen bonds, carbon–hydrogen bonds, and a π–donor hydrogen bond, with seven amino acid residues. Strong hydrogen bond interactions included PHE 564 (2.59 Å), THR 567 (3.38 Å and 3.32 Å), ARG 189 (3.03 Å), ASN 570 (3.26 Å), TYR 191 (3.05 Å), and ASP 243 (2.30 Å and 2.34 Å). Additional carbon–hydrogen bonds were observed at SER 566 (3.66 Å and 3.72 Å) and ASN 570 (4.19 Å), while a π-donor hydrogen bond was recorded at ASN 570 (3.19 Å). Wu *et al.*[14] similarly demonstrated that mangiferin interacts

Table 7 Docking analysis of mangiferin and acarbose with α-glucosidase

Ligand	Binding affinity (Vina score, kcal mol^{-1})	Interacting amino acids	Interaction type	Bond distance (Å)
Mangiferin	−8.0	PHE 564	Conventional hydrogen bond	2.59
		THR 567	Conventional hydrogen bond	3.38
		THR 567	Conventional hydrogen bond	3.32
		SER 566	Carbon–hydrogen bond	3.66
		SER 566	Carbon–hydrogen bond	3.72
		ARG 189	Conventional hydrogen bond	3.03
		ASN 570	Carbon–hydrogen bond	4.19
		ASN 570	Conventional hydrogen bond	3.26
		ASN 570	π–donor hydrogen bond	3.19
		TYR 191	Conventional hydrogen bond	3.05
		ASP 243	Conventional hydrogen bond	2.30
		ASP 243	Conventional hydrogen bond	2.34
Acarbose	−7.3	SER 560	Conventional hydrogen bond	2.93
		GLN 244	Conventional hydrogen bond	2.47
		GLY 334	Carbon–hydrogen bond	2.86
		ARG 190	Unfavourable donor–donor	1.89
		ASN 570	Conventional hydrogen bond	3.11
		ASP 243	Carbon–hydrogen bond	3.50
		ASP 243	Carbon–hydrogen bond	3.25

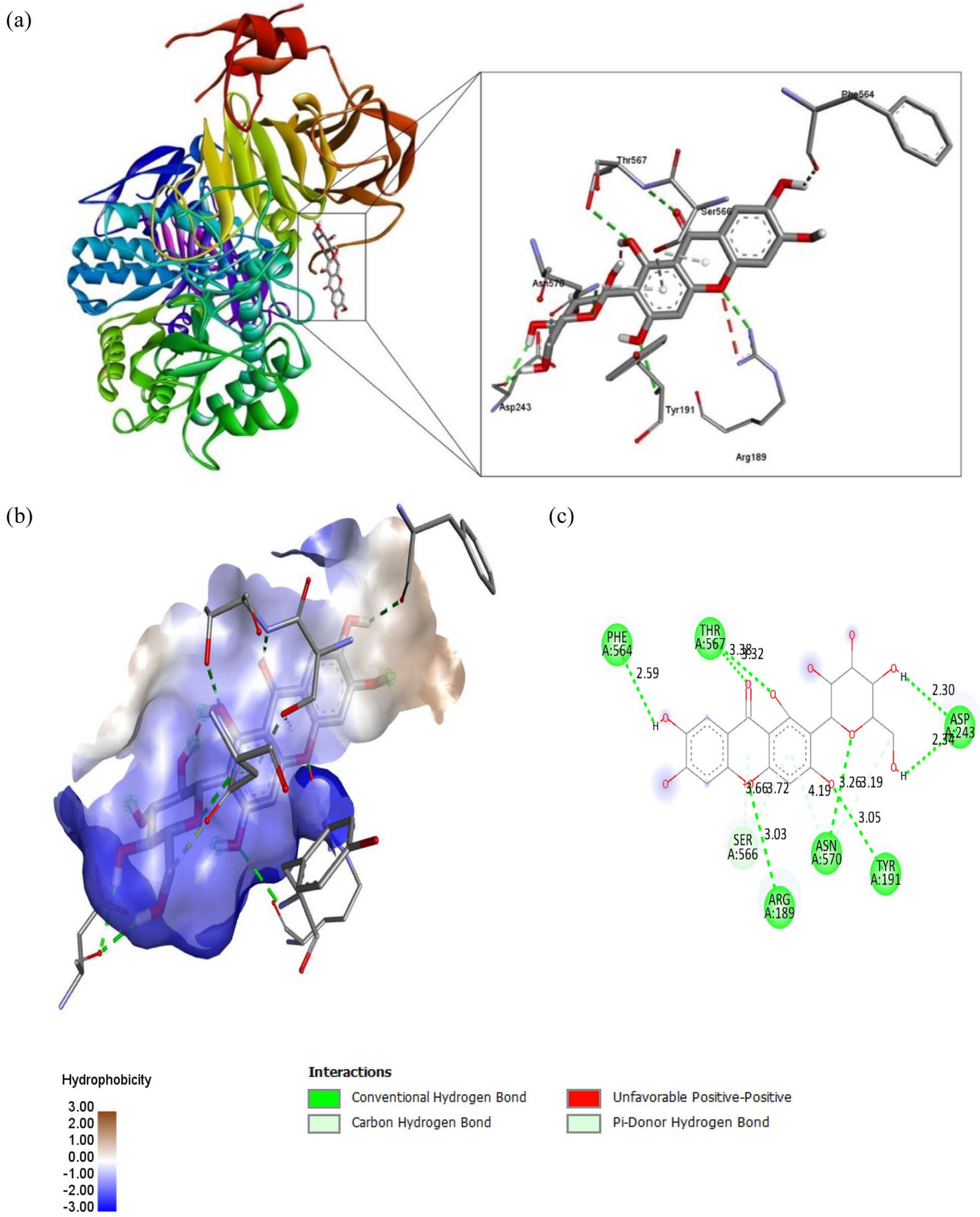

Fig. 10 Docking interactions of mangiferin–α-glucosidase (5NN8): (a) 3D amino acid interactions, (b) 3D hydrophobicity surface, and (c) 2D binding interactions of the docked complex.

with α-glucosidase at residues ASP 215, ARG 213, ARG 315, ARG 442, ARG 446, and ASN 415. In contrast, Fig. 11 shows that acarbose formed six hydrogen bond-related interactions with five amino acid residues, including conventional hydrogen bonds at SER 560 (2.93 Å), GLN 244 (2.47 Å), and ASN 570 (3.11 Å), as well as carbon–hydrogen bonds at GLY 334 (2.86 Å) and ASP 243 (3.50 Å and 3.25 Å). An unfavourable donor–donor interaction was observed at ARG 190 (1.89 Å). El-Sayed *et al.*[76] explained that unfavourable donor–donor interactions introduce repulsive forces between the ligand and protein, thereby

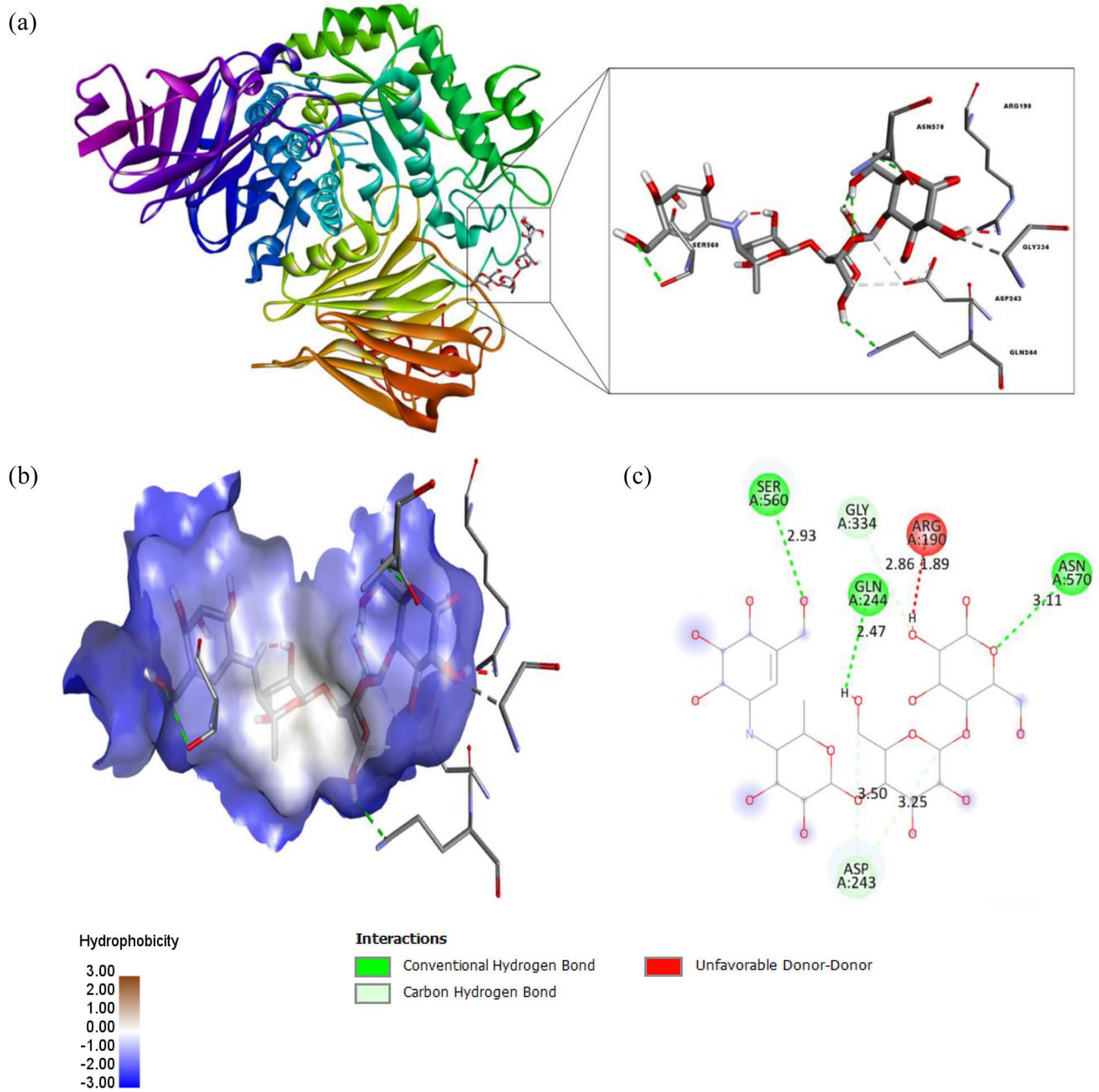

Fig. 11 Docking interactions of acarbose-α-glucosidase (5NN8): (a) 3D amino acid interactions, (b) 3D hydrophobicity surface, and (c) 2D binding interactions of the docked complex.

destabilising complex formation. Overall, mangiferin showed stronger binding to α-glucosidase than acarbose, as supported by its more negative binding affinity and greater number of stabilising interactions with key amino acid residues.[77,78]

3.5 ADMET and drug-likeness prediction of the optimised MPFE

ADMET analysis provides a preliminary insight into the potential pharmacokinetic behaviour of compounds and may support early-stage evaluation of their suitability for further study as bioactive agents. As shown in Table 8, mangiferin (0.544) demonstrated higher predicted human intestinal absorption (HIA) than acarbose (0.060), suggesting a greater likelihood of systemic absorption, whereas acarbose may remain more confined to the gastrointestinal tract. The blood–brain barrier (BBB) protects the brain from toxins and unwanted substances that can cause central nervous system side effects.[79] Mangiferin (0.122) exhibited lower predicted BBB penetration than acarbose (0.135), which may be favourable for an antidiabetic compound if reduced central nervous system exposure is preferred.[80,81] Both mangiferin and acarbose were predicted to be nonsubstrates and noninhibitors of CYP, suggesting a low likelihood of cytochrome P450-mediated metabolic interaction under the predicted conditions. Raju *et al.*[82] reported that diabetes can lead to kidney failure. Mangiferin showed higher renal clearance (CLr, 0.803) than acarbose (0.598), indicating more efficient renal processing. Both compounds were predicted to present a potentially low risk in the rat carcinogenicity model, although these findings

Table 8 ADMET prediction results for mangiferin and acarbose

Ligand	HIA	BBB	CYP substrate/inhibitor status	CLr	Carcinogenicity (rat model)
Mangiferin	0.544	0.122	Nonsubstrate/noninhibitor	0.803	Potentially low risk
Acarbose	0.060	0.135	Nonsubstrate/noninhibitor	0.598	Potentially low risk

Table 9 Drug-likeness prediction results for mangiferin and acarbose

	Ro5							
Ligand	MW (g mol^{-1})	HBD	HBA	c Log P	Ro5 violations	Log S	TPSA (Å^2)	Drug-likeness
Mangiferin	422.34	8	11	−0.43	2	−2.347	197.3	0.24
Acarbose	645.61	14	19	−7.91	3	−0.301	329.0	0.29

are based solely on computational prediction and require further experimental and *in vivo* validation.

Drug-likeness defines the qualities necessary for a compound to be considered a strong drug candidate.[83] Ro5 evaluates oral bioavailability based on MW < 500 g mol^{-1}, HBDs < 5, HBAs < 10, and c log P < 5, with no more than one violation.[84] As shown in Table 9, mangiferin violated two Ro5 criteria (8 HBDs > 5 and 11 HBAs > 10), while meeting the MW (422.34 g mol^{-1}) and c log P (−0.43) requirements. Acarbose violated three Ro5 criteria: MW (645.61 g mol^{-1} > 500), HBDs (14 > 5), and HBAs (19 > 10), while also showing a c log P of −7.91. These results suggest that mangiferin is more compliant with Ro5 compared with acarbose. Although mangiferin has relatively low bioavailability, formulation strategies such as nanoparticle encapsulation may improve absorption.[85] Solubility also affects drug potential, with compounds having log S < −2 considered soluble and log S < 0 considered very soluble.[86] Based on this criterion, acarbose (−0.301) was more soluble than mangiferin (−2.347). Prasetiawati *et al.*[87] stated that a TPSA below 140 Å^2 indicates good membrane permeability. Although mangiferin had a lower TPSA (197.3 Å^2) than acarbose (329.0 Å^2), both compounds exceeded this threshold, suggesting that membrane permeability may still be limited based on this criterion. In addition, the predicted drug-likeness values were 0.24 for mangiferin and 0.29 for acarbose, indicating only a small difference between the two ligands based on this descriptor. Taken together, these findings suggest that mangiferin may possess somewhat more favourable drug-likeness and ADMET-related properties than acarbose in certain respects. However, these results should be interpreted cautiously, as the findings are based on computational prediction and do not provide definitive evidence of therapeutic potential without further experimental and *in vivo* validation.

4 Conclusion

This study demonstrated the effectiveness of combining UAE with NADES to enhance the recovery of TPC, TFC, and mangiferin from UAOD-pretreated MPFE under optimised conditions of an extraction time of 11.33 min, solid-to-solvent ratio of 1 : 28.52 g mL^{-1}, and ultrasonic amplitude of 51.41%, yielding 53.02 ± 1.57 mg GAE g^{-1} TPC, 17.26 ± 1.13 mg RE g^{-1} TFC, and 0.66 ± 0.01 mg g^{-1} mangiferin. The IC_{50} values of optimised MPFE for DPPH (117.58 ± 2.19 μg mL^{-1}) and α-glucosidase (90.54 ± 1.60 μg mL^{-1}) indicated notable antioxidant and antidiabetic activities, although these activities were lower than those of positive controls. Molecular docking further showed that mangiferin exhibited stronger binding affinity towards α-glucosidase than acarbose. ADMET and drug-likeness prediction suggested that mangiferin may possess more favourable pharmacokinetic and drug-like properties than acarbose in certain respects. Overall, these findings highlight *M. pajang* fruit as a promising and sustainable natural source of antioxidant and antidiabetic compounds with potential applications in nutraceutical and functional food products. The use of UAE with NADES also suggests potential for industrial application due to the relatively short extraction time and the use of a green solvent system. However, further studies are needed to confirm process scalability, evaluate long-term stability, and validate the biological effects *in vivo*.

Author contributions

Muhammad Daniel Eazzat Mohd Rosdan: methodology, software, validation, formal analysis, investigation, data curation, writing – original draft, visualization; Mohd Azrie Awang: conceptualization, methodology, investigation, resources, writing – review & editing, supervision, project administration, funding acquisition; Mohammad Amil Zulhilmi Benjamin: formal analysis, writing – review & editing, visualization; Aniza Saini: validation, data curation; Muhammad Naufal Qaweim Rushdy: validation, data curation, visualization; Hasdian Mudin: validation, visualization.

Conflicts of interest

There are no conflicts to declare.

Data availability

Data will be made available on request.

Acknowledgements

The authors convey their appreciation to the Faculty of Food Science and Nutrition at Universiti Malaysia Sabah, Sabah, Malaysia, for their facility and financial support. This research was funded by Universiti Malaysia Sabah through the Skim Pensyarah Lantikan Baru (SLB2234).

References

1 J. K. U. Ling and K. Hadinoto, Deep eutectic solvent as green solvent in extraction of biological macromolecules: a review, *Int. J. Mol. Sci.*, 2022, **23**(6), 3381, DOI: 10.3390/ijms23063381.

2 H. Shekaari, M. T. Zafarani-Moattar and M. Mokhtarpour, Effective ultrasonic-assisted extraction and solubilization of curcuminoids from turmeric by using natural deep eutectic solvents and imidazolium-based ionic liquids, *J. Mol. Liq.*, 2022, **360**, 119351, DOI: 10.1016/j.molliq.2022.119351.

3 S. Milošević, A. Bebek Markovinović, N. Teslić, A. Mišan, M. Pojić, I. Brčić Karačonji, *et al.*, Use of natural deep eutectic solvent (NADES) as a green extraction of antioxidant polyphenols from strawberry tree fruit (*Arbutus unedo* L.): an optimization study, *Microchem. J.*, 2024, **200**, 110284, DOI: 10.1016/j.microc.2024.110284.

4 N. Vural, Ö. Algan Cavuldak and M. A. Akay, D-Optimal design and multi-objective optimization for green extraction conditions developed with ultrasonic probe for oleuropein, *J. Appl. Res. Med. Aromat. Plants*, 2021, **20**, 100279, DOI: 10.1016/j.jarmap.2020.100279.

5 M. W. R. Chy, T. Ahmed, J. Iftekhar, M. Z. Islam and M. R. Rana, Optimization of microwave-assisted polyphenol extraction and antioxidant activity from papaya peel using response surface methodology and artificial neural network, *Appl. Food Res.*, 2024, **4**(2), 100591, DOI: 10.1016/j.afres.2024.100591.

6 N. Szpisják-Gulyás, A. N. Al-Tayawi, Z. H. Horváth, Z. László, S. Kertész and C. Hodúr, Methods for experimental design, central composite design and the Box–Behnken design, to optimise operational parameters: a review, *Acta Aliment.*, 2023, **52**(4), 521–537, DOI: 10.1556/066.2023.00235.

7 F. S. Braim, N. N. A. Razak, A. A. Aziz, M. A. Dheyab and L. Q. Ismael, Optimization of ultrasonic-assisted approach for synthesizing a highly stable biocompatible bismuth-coated iron oxide nanoparticles using a face-centered central composite design, *Ultrason. Sonochem.*, 2023, **95**, 106371, DOI: 10.1016/j.ultsonch.2023.106371.

8 M. Li, M. Shahid, X. Zhang, D. Law, M. M. Mackeen, A. H. Teh, *et al.*, Extraction, chemical composition and antidiabetic potential of crude polysaccharides from *Centella asiatica* (L.) Urban, *Pol. J. Food Nutr. Sci.*, 2024, **74**(2), 177–187, DOI: 10.31883/pjfns/188316.

9 IDF, *IDF Diabetes Atlas, 9th Edition*, International Diabetes Federation, 2019, p. 168.

10 IDF, *IDF Diabetes Atlas, 11th Edition*, International Diabetes Federation, 2025, p. 125, https://diabetesatlas.org/resources/idf-diabetes-atlas-2025/.

11 B. M. Paul, G. Jagadeesan, G. Kannan, F. Jegan Raj, Y. Annadurai, S. Piramanayagam, *et al.*, Exploring the hypoglycaemic efficacy of bio-accessed antioxidative polyphenolics in thermally processed *Cucumis dipsaceus* fruits – an *in vitro* and *in silico* study, *Food Chem.*, 2024, **435**, 137577, DOI: 10.1016/j.foodchem.2023.137577.

12 N. Nasim, I. S. Sandeep and S. Mohanty, Plant-derived natural products for drug discovery: current approaches and prospects, *Nucleus*, 2022, **65**(3), 399–411, DOI: 10.1007/s13237-022-00405-3.

13 M. H. A. Jahurul, I. S. M. Zaidul, L. Beh, M. S. Sharifudin, S. Siddiquee, M. Hasmadi, *et al.*, Valuable components of bambangan fruit (*Mangifera pajang*) and its co-products: a review, *Food Res. Int.*, 2019, **115**, 105–115, DOI: 10.1016/j.foodres.2018.08.017.

14 L. Wu, W. Wu, Y. Cai, C. Li and L. Wang, HPLC fingerprinting-based multivariate analysis of phenolic compounds in mango leaves varieties: correlation to their antioxidant activity and *in silico* α-glucoidase inhibitory ability, *J. Pharm. Biomed. Anal.*, 2020, **191**, 113616, DOI: 10.1016/j.jpba.2020.113616.

15 F. A. Hassan, A. Ismail, A. Abdulhamid and A. Azlan, Identification and quantification of phenolic compounds in bambangan (*Mangifera pajang* Kort.) peels and their free radical scavenging activity, *J. Agric. Food Chem.*, 2011, **59**(17), 9102–9111, DOI: 10.1021/jf201270n.

16 N. F. Lasano, N. S. Ramli, A. Abdul Hamid, R. Karim, M. S. Pak Dek and F. Abas, *In vitro* antidiabetic property and phytochemical profiling of *Mangifera odorata* pulp using UHPLC-ESI-Orbitrap-MS/MS, *Int. Food Res. J.*, 2021, **28**(2), 366–376, DOI: 10.47836/ifrj.28.2.18.

17 F. Salehi, Recent advances in the ultrasound-assisted osmotic dehydration of agricultural products: a review, *Food Biosci.*, 2023, **51**, 102307, DOI: 10.1016/j.fbio.2022.102307.

18 M. D. E. Mohd Rosdan, M. A. Awang, M. A. Z. Benjamin, S. F. Mohd Amin and N. Julmohammad, Effect of ultrasound-assisted osmotic dehydration (UAOD) pretreatment on *Mangifera pajang* Kosterm. fruit pulp: drying kinetics, chemical qualities, and color measurement, *J. Food Process Eng.*, 2024, **47**(9), e14721, DOI: 10.1111/jfpe.14721.

19 F. R. Abrahão, J. L. G. Corrêa, A. D. E. B. M. Sousa, P. G. Silveira and R. N. da Cunha, Effect of ultrasound and osmotic dehydration as pretreatments on the infrared drying of banana slices, *Food Technol. Biotechnol.*, 2024, **62**(3), 384–396, DOI: 10.17113/ftb.62.03.24.8409.

20 G. Ozkan, Valorization of artichoke outer petals by using ultrasound-assisted extraction and natural deep eutectic solvents (NADES) for the recovery of phenolic compounds, *J. Sci. Food Agric.*, 2024, **104**(5), 2744–2749, DOI: 10.1002/jsfa.13158.

21 M. Z. A. Zulkifli, M. A. Z. Benjamin, M. D. E. Mohd Rosdan, A. Saini, N. A. Rusdi and M. A. Awang, Optimisation of yield, flavonoids, and antioxidant activity *via* ultrasound-assisted extraction of bamboo leaves from *Dinochloa sublaevigata* S.

Dransf. (wadan) in Sabah, Malaysia, *Adv. Bamboo Sci.*, 2025, **10**, 100128, DOI: 10.1016/j.bamboo.2025.100128.

22 A. A. Alfaleh and H. A. Sindi, Systematic study on date palm seeds (*Phoenix dactylifera* L.) extraction optimisation using natural deep eutectic solvents and ultrasound technique, *Sci. Rep.*, 2024, **14**(1), 16622, DOI: 10.1038/s41598-024-67416-9.

23 B. Sik, Z. Ajtony, E. Lakatos and R. Székelyhidi, Wild blackberry fruit (*Rubus fruticosus* L.) as potential functional ingredient in food: ultrasound-assisted extraction optimization, ripening period evaluation, application in muffin, and consumer acceptance, *Foods*, 2024, **13**(5), 666, DOI: 10.3390/foods13050666.

24 R. Rashid, S. Mohd Wani, S. Manzoor, F. A. Masoodi and M. Masarat Dar, Green extraction of bioactive compounds from apple pomace by ultrasound assisted natural deep eutectic solvent extraction: optimisation, comparison and bioactivity, *Food Chem.*, 2022, **398**, 133871, DOI: 10.1016/j.foodchem.2022.133871.

25 K. J. Lanjekar, S. Gokhale and V. K. Rathod, Utilization of waste mango peels for extraction of polyphenolic antioxidants by ultrasound-assisted natural deep eutectic solvent, *Bioresour. Technol. Rep.*, 2022, **18**, 101074, DOI: 10.1016/j.biteb.2022.101074.

26 A. A. Bin Mokaizh, A. H. Nour and K. Kerboua, Ultrasonic-assisted extraction to enhance the recovery of bioactive phenolic compounds from *Commiphora gileadensis* leaves, *Ultrason. Sonochem.*, 2024, **105**, 106852, DOI: 10.1016/j.ultsonch.2024.106852.

27 I. Egüés, F. Hernandez-Ramo, I. Rivilla and J. Labidi, Optimization of ultrasound assisted extraction of bioactive compounds from apple pomace, *Molecules*, 2021, **26**(13), 3783, DOI: 10.3390/molecules26133783.

28 K. Kumar, S. Srivastav and V. S. Sharanagat, Ultrasound assisted extraction (UAE) of bioactive compounds from fruit and vegetable processing by-products: a review, *Ultrason. Sonochem.*, 2021, **70**, 105325, DOI: 10.1016/j.ultsonch.2020.105325.

29 H. Mudin, M. A. Z. Benjamin, M. A. Awang, M. N. Q. Rushdy, M. D. E. Mohd Rosdan, A. Saini and D. Setijawati, Green solvent-based extraction of *Annona muricata* L. (soursop) leaves: influence on physicochemical properties, phytochemical content, and antioxidant activity, *Innov. Food Technol.*, 2026, **13**(3), 223–233, DOI: 10.22104/ift.2025.8033.2257.

30 N. A. Z. Jinin, M. A. Z. Benjamin and M. A. Awang, Drying kinetics and quality assessment of noodles from *Piper sarmentosum* Roxb. (kaduk) leaves, *Malaysian J. Fundam. Appl. Sci.*, 2024, **20**(4), 835–851, DOI: 10.11113/mjfas.v20n4.3519.

31 A. Saini, M. A. Z. Benjamin, M. D. E. Mohd Rosdan, M. N. Mohamad Rosdi and M. A. Awang, Phenolic and chlorogenic acid recovery from *Solanum lasiocarpum* Dunal (terung asam) *via* solid-phase extraction: fractionation, antioxidant, molecular docking, and anti-obesity, *Malays. J. Anal. Sci.*, 2025, **29**(3), 1460.

32 C. Lankatillake, S. Luo, M. Flavel, G. B. Lenon, H. Gill, T. Huynh, *et al.*, Screening natural product extracts for potential enzyme inhibitors: protocols, and the standardisation of the usage of blanks in α-amylase, α-glucosidase and lipase assays, *Plant Methods*, 2021, **17**(1), 3, DOI: 10.1186/s13007-020-00702-5.

33 M. Z. Sabri, M. A. Awang, A. A. Hamzah, K. F. Pa'ee and K. Y. T. Len, *In silico* molecular and dynamic analysis of biomarkers against cordycepin from *Cordyceps militaris* in colorectal cancer, *AIP Conf. Proc.*, 2024, **2923**(1), 30005, DOI: 10.1063/5.0195504.

34 B. K. Sarkar, M. J. I. Polash, M. J. Islam, M. A. Hanif, N. Jannat, S. K. Kund, *et al.*, Unlocking the therapeutic potential of *Catharanthus roseus* leaves *via in vitro*, *in vivo*, and *in silico* study, *Sci. Rep.*, 2025, **15**(1), 25909, DOI: 10.1038/s41598-025-96643-x.

35 M. N. Mohamad Rosdi and F. Husin, Elucidation of stilbene-derivatives as potential inhibitors of SARS-CoV-2 M^{pro} binding pocket: a molecular docking, and ADMET prediction studies, *Int. J. Food*, 2024, **1**(1), 56–68, DOI: 10.51200/ijf.v1i1.4898.

36 E. E. Asanga, C. M. Ekeleme, I. E. Udoh, A. N. Inyang, P. S. Thomas, A. P. Joseph, *et al.*, Exploring anti-diabetic activity of *Xylopia aethiopica* compounds as potential inhibitors of α-amylase and α-glucosidase: experimental and computational approach, *Nat. Prod. Commun.*, 2025, **20**(3), 1–13, DOI: 10.1177/1934578X251325717.

37 J. O. Chaves, M. C. de Souza, L. C. da Silva, D. Lachos-Perez, P. C. Torres-Mayanga, A. P. D. A. F. Machado, *et al.*, Extraction of flavonoids from natural sources using modern techniques, *Front. Chem.*, 2020, **8**, 507887, DOI: 10.3389/fchem.2020.507887.

38 H. Aktaş and M. A. Kurek, Deep eutectic solvents for the extraction of polyphenols from food plants, *Food Chem.*, 2024, **444**, 138629, DOI: 10.1016/j.foodchem.2024.138629.

39 D. M. B. Ginting, D. A. Suroto and R. Millati, Optimization of ultrasound-assisted pectin extraction from durian rind, *J. Appl. Sci. Eng.*, 2025, **28**(2), 367–380, DOI: 10.6180/jase.202502_28(2).0015.

40 M. D. E. Mohd Rosdan, M. A. Awang, M. A. Z. Benjamin, F. A. Andrew, A. Saini, S. F. Mohd Amin, *et al.*, Natural deep eutectic solvents *vs.* conventional solvents: effects on crude yield, mangiferin content, antioxidant activity, and toxicity in *Mangifera pajang* Kosterm. fruit extracts, *Malays. Appl. Biol.*, 2025, **54**(1), 87–97, DOI: 10.55230/mabjournal.v54i1.3212.

41 V. B. Thakare, G. C. Jadeja and M. A. Desai, Extraction of mangiferin and pectin from mango peels using process intensified tactic: a step towards waste valorization, *Chem. Eng. Res. Des.*, 2023, **192**, 280–288, DOI: 10.1016/j.cherd.2023.02.036.

42 Y. A. Bhadange, V. K. Saharan, S. H. Sonawane and G. Boczkaj, Intensification of catechin extraction from the bark of *Syzygium cumini* using ultrasonication: optimization, characterization, degradation analysis and kinetic studies, *Chem. Eng. Process. Process Intensif.*, 2022, **181**, 109147, DOI: 10.1016/j.cep.2022.109147.

43 C. S. Dzah, Y. Duan, H. Zhang, C. Wen, J. Zhang, G. Chen, *et al.*, The effects of ultrasound assisted extraction on yield, antioxidant, anticancer and antimicrobial activity of polyphenol extracts: a review, *Food Biosci.*, 2020, **35**, 100547, DOI: 10.1016/j.fbio.2020.100547.

44 W. Wang, Y. Pan, J. Zhao, Y. Wang, Q. Yao and S. Li, Development and optimization of green extraction of polyphenols in *Michelia alba* using natural deep eutectic solvents (NADES) and evaluation of bioactivity, *Sustain. Chem. Pharm.*, 2024, **37**, 101425, DOI: 10.1016/j.scp.2023.101425.

45 M. Pattnaik, P. Pandey, G. J. O. Martin, H. N. Mishra and M. Ashokkumar, Innovative technologies for extraction and microencapsulation of bioactives from plant-based food waste and their applications in functional food development, *Foods*, 2021, **10**(2), 279, DOI: 10.3390/foods10020279.

46 S. S. Patil, A. Pathak and V. K. Rathod, Optimization and kinetic study of ultrasound assisted deep eutectic solvent based extraction: a greener route for extraction of curcuminoids from *Curcuma longa*, *Ultrason. Sonochem.*, 2021, **70**, 105267, DOI: 10.1016/j.ultsonch.2020.105267.

47 K. V. Mahindrakar and V. K. Rathod, Ultrasonic assisted aqueous extraction of catechin and gallic acid from *Syzygium cumini* seed kernel and evaluation of total phenolic, flavonoid contents and antioxidant activity, *Chem. Eng. Process. Process Intensif.*, 2020, **149**, 107841, DOI: 10.1016/j.cep.2020.107841.

48 Z. Kobus, M. Krzywicka, A. Starek-Wójcicka and A. Sagan, Effect of the duty cycle of the ultrasonic processor on the efficiency of extraction of phenolic compounds from *Sorbus intermedia*, *Sci. Rep.*, 2022, **12**(1), 8311, DOI: 10.1038/s41598-022-12244-y.

49 S. S. Patil and V. K. Rathod, Synergistic effect of ultrasound and three phase partitioning for the extraction of curcuminoids from *Curcuma longa* and its bioactivity profile, *Process Biochem.*, 2020, **93**, 85–93, DOI: 10.1016/j.procbio.2020.02.031.

50 Z. Khoshraftar, H. Masoumi and A. Ghaemi, Experimental, response surface methodology (RSM) and mass transfer modeling of heavy metals elimination using dolomite powder as an economical adsorbent, *Case Stud. Chem. Environ. Eng.*, 2023, **7**, 100329, DOI: 10.1016/j.cscee.2023.100329.

51 K. N. Abhini, A. B. Rajan, K. F. Zuhara and D. Sebastian, Response surface methodological optimization of L-asparaginase production from the medicinal plant endophyte *Acinetobacter baumannii* ZAS1, *J. Genet. Eng. Biotechnol.*, 2022, **20**(1), 22, DOI: 10.1186/s43141-022-00309-4.

52 D. Susanti, F. S. Ruslan, M. I. Shukor, N. M. Nor, N. I. Aminudin, M. Taher, *et al.*, Optimisation of vitamin B12 extraction from green edible seaweed (*Ulva lactuca*) by applying the central composite design, *Molecules*, 2022, **27**(14), 4459, DOI: 10.3390/molecules27144459.

53 H. Benmoussa, I. Béchohra, S. He, W. Elfalleh and R. Chawech, Optimization of sonohydrodistillation and microwave assisted hydrodistillation by response surface methodology for extraction of essential oils from *Cinnamomum cassia* barks, *Ind. Crops Prod.*, 2023, **192**, 115995, DOI: 10.1016/j.indcrop.2022.115995.

54 M. Alsawalha, An approach utilizing the response surface methodology (RSM) to optimize adsorption-desorption of natural Saudi Arabian diatomite with the Box–Behnken design technique, *Arab. J. Chem.*, 2023, **16**(1), 104413, DOI: 10.1016/j.arabjc.2022.104413.

55 E. A. Bekele, H. A. Korsa and Y. M. Desalegn, Electrolytic synthesis of γ-Al_2O_3 nanoparticle from aluminum scrap for enhanced methylene blue adsorption: experimental and RSM modeling, *Sci. Rep.*, 2024, **14**(1), 16957, DOI: 10.1038/s41598-024-67656-9.

56 P. Saetiao, N. Kongrit, J. Jitjamnong, C. Direksilp, C. K. Cheng and N. Khantikulanon, Enhancing sustainable production of fatty acid methyl ester from palm oil using bio-based heterogeneous catalyst: process simulation and techno-economic analysis, *ACS Omega*, 2023, **8**(33), 30598–30611, DOI: 10.1021/acsomega.3c04209.

57 R. N. Gavril, O. E. Constantin, E. Enachi, F. Stoica, F. D. Lipșa, N. Stănciuc, *et al.*, Optimization of the parameters influencing the antioxidant activity and concentration of carotenoids extracted from pumpkin peel using a central composite design, *Plants*, 2024, **13**(11), 1447, DOI: 10.3390/plants13111447.

58 A. Dobrinčić, M. Repajić, I. Elez Garofulić, L. Tuđen, V. Dragović-Uzelac and B. Levaj, Comparison of different extraction methods for the recovery of olive leaves polyphenols, *Processes*, 2020, **8**(9), 1008, DOI: 10.3390/pr8091008.

59 L. M. Anaya-Esparza, E. F. Aurora-Vigo, Z. Villagrán, E. Rodríguez-Lafitt, J. M. Ruvalcaba-Góme, M. Á. Solano-Cornejo, V. M. Zamora-Gasga, E. Montalvo-González, H. Gómez-Rodríguez, C. E. Aceves-Aldrete and N. González-Silva, Design of experiments for optimizing ultrasound-assisted extraction of bioactive compounds from plant-based sources, *Molecules*, 2023, **28**(23), 7752, DOI: 10.3390/molecules28237752.

60 R. C. Lima, A. P. A. de Carvalho, B. D. da Silva, L. T. Neto, M. R. D. A. S. de Figueiredo, P. H. T. Chaves, A. E. C. C. de Almeida and C. A. Conte-Junior, Green ultrasound-assisted extraction of bioactive compounds of babassu (*Attalea speciosa*) mesocarp: effects of solid-liquid ratio extraction, antioxidant capacity, and antimicrobial activity, *Appl. Food Res.*, 2023, **3**(2), 100331, DOI: 10.1016/j.afres.2023.100331.

61 V. Hiranpradith, N. Therdthai, A. Soontrunnarudrungsri and O. Rungsuriyawiboon, Optimisation of ultrasound-assisted extraction of total phenolics and flavonoids content from Centella asiatica, *Foods*, 2025, **14**(2), 291, DOI: 10.3390/foods14020291.

62 F. L. Garcia-Larez, J. Esquer, H. Guzmán, D. S. Zepeda-Quintana, M. J. Moreno-Vásquez, F. Rodríguez-Félix, C. L. Del-Toro-Sánchez, B. E. López-Corona and J. A. Tapia-Hernández, Effect of ultrasound-assisted extraction (UAE) parameters on the recovery of polyphenols from pecan nutshell waste biomass and its antioxidant activity,

Biomass Convers. Biorefinery, 2025, **15**(7), 10977–10995, DOI: 10.1007/s13399-024-05901-x.

63 P. Mehganathan, N. A. Rosli, K. Abd Karim and T. Soon Huat, Optimizing quercetin and kaempferol extraction from Moringa oleifera leaves via ultrasonic assisted extraction: kinetic modeling and process optimization, *J. Eng. Res.*, 2025, **13**(3), 2432–2444, DOI: 10.1016/j.jer.2024.06.022.

64 H. Xue, J. Tan, Q. Li, J. Tang and X. Cai, Optimization ultrasound-assisted deep eutectic solvent extraction of anthocyanins from raspberry using response surface methodology coupled with genetic algorithm, *Foods*, 2020, **9**(10), 1409, DOI: 10.3390/foods9101409.

65 A. Patra, S. Abdullah and R. C. Pradhan, Application of artificial neural network-genetic algorithm and response surface methodology for optimization of ultrasound-assisted extraction of phenolic compounds from cashew apple bagasse, *J. Food Process Eng.*, 2021, **44**(10), e13828, DOI: 10.1111/jfpe.13828.

66 C. Moldovan, A. Nicolescu, O. Frumuzachi, G. Rocchetti, L. Lucini, A. Mocan and G. Crișan, Ultrasound-assisted sustainable extraction of bioactive phytochemicals in shallot (*Allium ascalonicum* L.) peel: a DoE and metabolomics combined approach, *Sustain. Chem. Pharm.*, 2024, **41**, 101729, DOI: 10.1016/j.scp.2024.101729.

67 A. Becze, V. L. Babalau-Fuss, C. Varaticeanu and C. Roman, Optimization of high-pressure extraction process of antioxidant compounds from *Feteasca regala* leaves using response surface methodology, *Molecules*, 2020, **25**(18), 4209, DOI: 10.3390/molecules25184209.

68 M. H. Mahnashi, Y. S. Alqahtani, A. O. Alqarni, B. A. Alyami, O. S. Alqahtani, M. S. Jan, *et al.*, Phytochemistry, anti-diabetic and antioxidant potentials of *Allium consanguineum* Kunth, *BMC Complement. Med. Ther.*, 2022, **22**(1), 154, DOI: 10.1186/s12906-022-03639-5.

69 R. S. Yehia and S. A. Altwaim, An insight into *in vitro* antioxidant, antimicrobial, cytotoxic, and apoptosis induction potential of mangiferin, a bioactive compound derived from *Mangifera indica*, *Plants*, 2023, **12**(7), 1539, DOI: 10.3390/plants12071539.

70 V. Sekar, S. Chakraborty, S. Mani, V. K. Sali and H. R. Vasanthi, Mangiferin from *Mangifera indica* fruits reduces post-prandial glucose level by inhibiting α-glucosidase and α-amylase activity, *S. Afr. J. Bot.*, 2019, **120**, 129–134, DOI: 10.1016/j.sajb.2018.02.001.

71 M. Khalid, M. H. Alqarni, A. Alsayari, A. I. Foudah, T. M. Aljarba, M. Mukim, *et al.*, Anti-diabetic activity of bioactive compound extracted from *Spondias mangifera* fruit: *in vitro* and molecular docking approaches, *Plants*, 2022, **11**(4), 562, DOI: 10.3390/plants11040562.

72 A. Maalaoui, E. C. Agwamba, H. Louis, G. E. Mathias, M. Rzaigui and S. Akriche, Combined experimental and computational study of V-substituted Lindqvist polyoxotungstate: screening by docking for potential antidiabetic activity, *Inorg. Chem.*, 2023, **62**(35), 14279–14290, DOI: 10.1021/acs.inorgchem.3c01651.

73 M. R. Islam, A. R. Haque, M. R. Kabir, M. M. Hasan, K. J. Khushe and S. M. K. Hasan, Fruit by-products: the potential natural sources of antioxidants and α-glucosidase inhibitors, *J. Food Sci. Technol.*, 2021, **58**(5), 1715–1726, DOI: 10.1007/s13197-020-04681-2.

74 S. Yakoubi, Enhancing plant-based cheese formulation through molecular docking and dynamic simulation of tocopherol and retinol complexes with zein, soy and almond proteins *via* SVM-machine learning integration, *Food Chem.*, 2024, **452**, 139520, DOI: 10.1016/j.foodchem.2024.139520.

75 Y.-C. Chu, C.-S. Yang, M.-J. Cheng, S.-L. Fu and J.-J. Chen, Comparison of various solvent extracts and major bioactive components from *Portulaca oleracea* for antioxidant, anti-tyrosinase, and anti-α-glucosidase activities, *Antioxidants*, 2022, **11**(2), 385, DOI: 10.3390/antiox11020398.

76 D. S. El-Sayed, S. S. Hassan, L. S. Jassim, A. A. Issa, F. AL-Oqaili, M. K. Albayaty, *et al.*, Structural and topological analysis of thiosemicarbazone-based metal complexes: computational and experimental study of bacterial biofilm inhibition and antioxidant activity, *BMC Chem.*, 2025, **19**(1), 24, DOI: 10.1186/s13065-024-01338-5.

77 C. Demir and E. S. Istifli, Docking-based virtual screening, ADMET, and network pharmacology prediction of anthocyanidins against human alpha-amylase and alpha-glucosidase enzymes as potential antidiabetic agents, *Int. J. Plant Based Pharm.*, 2022, **2**(2), 271–283, DOI: 10.29228/ijpbp.9.

78 C. Ma, J. Lu, M. Ren, Q. Wang, C. Li, X. Xi, *et al.*, Rapid identification of α-glucosidase inhibitors from *Poria* using spectrum-effect, component knock-out, and molecular docking technique, *Front. Nutr.*, 2023, **10**(1), 1089829, DOI: 10.3389/fnut.2023.1089829.

79 K. Gandla, F. Islam, M. Zehravi, A. Karunakaran, I. Sharma, M. A. Haque, *et al.*, Natural polymers as potential P-glycoprotein inhibitors: pre-ADMET profile and computational analysis as a proof of concept to fight multidrug resistance in cancer, *Heliyon*, 2023, **9**(9), e19454, DOI: 10.1016/j.heliyon.2023.e19454.

80 A. M. Udrea, G. Gradisteanu Pircalabioru, A. A. Boboc, C. Mares, A. Dinache, M. Mernea, *et al.*, Advanced bioinformatics tools in the pharmacokinetic profiles of natural and synthetic compounds with anti-diabetic activity, *Biomolecules*, 2021, **11**(11), 1692, DOI: 10.3390/biom11111692.

81 N. M. Abdelazeem, W. M. Aboulthana, A. S. Hassan, A. A. Almehizia, A. M. Naglah and H. M. Alkahtani, Synthesis, *in silico* ADMET prediction analysis, and pharmacological evaluation of sulfonamide derivatives tethered with pyrazole or pyridine as anti-diabetic and anti-Alzheimer's agents, *Saudi Pharm. J.*, 2024, **32**(5), 102025, DOI: 10.1016/j.jsps.2024.102025.

82 R. Raju, I. Prabath, I. Chandrasekaran and S. Varadarajan, Dorzagliatin: a breakthrough glucokinase activator coming on board to treat diabetes mellitus, *Cureus*, 2024, **16**(7), e65708, DOI: 10.7759/cureus.65708.

83 N. B. Maulydia, K. Khairan, T. E. Tallei, S. Salaswati, A. Musdalifah, F. F. Nabila, *et al.*, Exploring the medicinal potential of *Blumea balsamifera*: insights from molecular docking and molecular dynamics simulations analyses, *Malacca Pharm.*, 2024, **2**(1), 33–40, DOI: 10.60084/mp.v2i1.168.

84 S. I. Khalivulla, A. U. R. Sankar and A. B. V. K. Kumar, Molecular docking studies of 3a,4-dihydro-3H-[1,3,2]oxazaphospholo[3,4-a]indole-1-oxide derivatives for anticancer activity, *J. Mol. Chem.*, 2024, **4**(2), 697.

85 S. Mei, M. Perumal, M. Battino, D. D. Kitts, J. Xiao, H. Ma, *et al.*, Mangiferin: a review of dietary sources, absorption, metabolism, bioavailability, and safety, *Crit. Rev. Food Sci. Nutr.*, 2023, **63**(18), 3046–3064, DOI: 10.1080/10408398.2021.1983767.

86 S. P. C. kurmi, S. Thapa, S. M. Metri, M. S. Biradar, V. A. Esther, A. K. Murav, *et al.*, Molecular docking, drug-likeness properties, and toxicity prediction of alkaloidal phytoconstituents of *Piper longum* against monoamine oxidase enzyme-A as an anti-depressive agent, *Discov. Chem.*, 2025, **2**(1), 105, DOI: 10.1007/s44371-025-00188-x.

87 R. Prasetiawati, E. N. Febrianti, S. Hamdani, N. K. K. Ikram, T. M. Fakih, D. Novitasari, *et al.*, Alpha-mangostin from *Garcinia mangostana* L.: a potential Nrf2 inhibitor for long COVID-19 explored through molecular dynamics, *J. Pharm. Pharmacogn. Res.*, 2025, **13**(2), 381–392, DOI: 10.56499/jppres24.2066_13.2.381.